Computational Cardiovascular Medicine With Isogeometric Analysis

Kenji TAKIZAWA[1,*], *Yuri BAZILEVS*[2], *Tayfun E. TEZDUYAR*[3,1], *Ming-Chen HSU*[4], *Takuya TERAHARA*[1]

[1]Waseda University, Tokyo, Japan
[2]Brown University, Providence, Rhode Island, USA
[3]Rice University, Houston, Texas, USA
[4]Iowa State University, Ames, Iowa, USA

*Corresponding Author: Kenji TAKIZAWA (Email: Kenji.Takizawa@tafsm.org)
(Received: 12-May-2022; accepted: 7-Jul-2022; published: 30-Sep-2022)
DOI: http://dx.doi.org/10.55579/jaec.202263.381

Abstract. *Isogeometric analysis (IGA) brought superior accuracy to computations in both fluid and solid mechanics. The increased accuracy has been in representing both the problem geometry and the variables computed. Beyond using IGA basis functions in space, with IGA basis functions in time in a space–time (ST) context, we can have increased accuracy also in representing the motion of solid surfaces. Around the core methods such as the residual-based variational multiscale (VMS), ST-VMS and arbitrary Lagrangian–Eulerian VMS methods, with complex-geometry IGA mesh generation methods and immersogeometric analysis, and with special methods targeting specific classes of computations, the IGA has been very effective in computational cardiovascular medicine. We provide an overview of these IGA-based computational-cardiovascular-medicine methods and present examples of the computations performed.*

Keywords

Computational cardiovascular medicine, Isogeometric analysis, Variational multiscale methods, Space–time method, ALE method, Complex-geometry IGA mesh generation methods, Immersogeometric analysis.

1. Introduction

The challenges involved in computational cardiovascular medicine (see, for example, [1–21]) include complex geometries, fluid–structure interaction (FSI) between the blood and the cardiovascular tissues, and topology changes in the computational domain, such as the contact between the heart valve leaflets. Because validation by comparing to experimental or test data is exceedingly difficult in many cases, striving for the best accuracy in all aspects of the computation is even more important. For example, as early as in 2004, with some of the earliest patient-specific arterial FSI computations [22, 23], which were performed with the Deforming-Spatial-Domain/Stabilized Space–Time (DSD/SST) method [24–26], it was shown that taking the FSI into account was essential for accurate prediction of the wall shear stress (WSS). The patient-specific arterial geometries used in [22, 23] were for the middle cerebral artery and internal carotid artery, and assuming rigid arteries was overpredicting the

WSS by large margins. The WSS overprediction trend was also reported in [27], with patient-specific arterial FSI computation for 10 different cases of cerebral aneurysm, with reasonably good boundary layer resolution near the arterial walls. As another example, the WSS significance of having a good boundary layer resolution near the arterial wall in finite element FSI computations was pointed out [28] and quantified [29] as early as in 2008.

Isogeometric analysis (IGA) [30–33] brought superior accuracy to computations in both fluid and solid mechanics. The increased accuracy has been in representing both the problem geometry and the variables computed. Beyond using IGA basis functions in space, with IGA basis functions in time in an ST context [34–37], we can have increased accuracy also in representing the motion of solid surfaces. The IGA has been used around core methods such as the residual-based variational multiscale (RBVMS) [38–41], arbitrary Lagrangian–Eulerian VMS (ALE-VMS) [1, 4,32,42–45], DSD/SST [24–26], which gained the alternate name "ST-SUPS" in [4], and ST-VMS [34, 35, 46]. It is known that IGA mesh generation for complex geometries is significantly more challenging than finite element mesh generation. This challenge has mostly been overcome or circumvented with the Complex-Geometry IGA Mesh Generation (CGIMG)[1] method [47, 48], NURBS Surface-to-Volume Guided Mesh Generation (NSVGMG) method [49], and immersogeometric analysis (IMGA) [11, 50]. With the core methods, with the methods that overcome or circumvent the complex-geometry IGA mesh generation challenge, and with special methods targeting specific classes of computations, the IGA has been very effective in computational cardiovascular medicine. We provide an overview of these IGA-based computational-cardiovascular-medicine methods and present examples of the computations performed. The overview of the methods is in Sections 2–12, and the examples are in Sections 13–15. The concluding remarks are given in Section 16.

[1]The method name and abbreviation are being coined here.

2. Moving-mesh and nonmoving-mesh methods

Flows with moving boundaries and interfaces (MBI) [4,51–53] is a wider class of flow problems that includes FSI problems. It also includes flows with moving mechanical components, free-surface and two fluid-flows, and fluid–particle interactions. For a given moving boundary or interface, if the method is relying on a mesh that moves to follow that boundary or interface, it is a moving-mesh method, if not, it is a nonmoving-mesh method[2]. Moving the mesh to follow a fluid–solid interface gives us mesh resolution control near the moving solid surfaces and higher accuracy in representing the boundary layers. The moving-mesh methods have also been referred to as "interface-tracking methods" [4, 51–54], meaning that the mesh is moving for the purpose of "tracking" the interface, rather than just "capturing" it within the mesh resolution where the interface is in the nonmoving mesh. More on the moving-mesh and nonmoving-mesh (i.e. interface-tracking and interface-capturing) methods and their mixtures, the Mixed Interface-Tracking/Interface-Capturing Technique [55] and Fluid–Solid Interface-Tracking/Interface-Capturing Technique (FSITICT) [56], can be found in [4, 51–53].

3. ST-SUPS, ALE-SUPS, RBVMS, ALE-VMS, ST-VMS, and the classes of problems computed

The ST-SUPS, introduced in 1990 with the name DSD/SST, is the oldest one of the

[2]We note that, in a flow computation in general, a method might be relying on a mesh that moves to follow a moving boundary or interface but does not move to follow a second moving boundary or interface. Then the method is a moving-mesh method for the first moving boundary or interface and a nonmoving-mesh method for the second.

moving-mesh methods we include in this article. The alternate name "ST-SUPS" brought clarity to the stabilization components, which are the SUPG and PSPG, with widespread awareness that these two acronyms imply stabilization methods Streamline-Upwind/Petrov-Galerkin [57] and Pressure-Stabilizing/Petrov-Galerkin [24]. The ram-air parachute FSI analysis in 1999 [58] was one of the earliest computations with the ALE-SUPS moving-mesh method. The root moving-mesh method ALE is of course much older, with the finite element version dating back to 1981 [59]. The ALE-VMS and ST-VMS are the VMS versions of the ALE and DSD/SST. In both, the stabilization components are from the RBVMS.

The ST-SUPS, ALE-SUPS, ALE-VMS, and ST-VMS, like all moving-mesh methods, need to be complemented with mesh update methods in FSI and MBI computations. The mesh update most of the time consists of moving the mesh to accommodate the motion of the boundaries and interfaces and to control the mesh resolution near solid surfaces that are moving, and remeshing if the element distortion exceeds an acceptable level. We expect two things from a good mesh moving method: to reduce the need for remeshing and to give high priority to maintaining element quality near solid surfaces where accurate representation of the boundary layers matters. Since the inception of the ST-SUPS in 1990, a large number of special- and general-purpose mesh moving methods have been developed for computations with the ST-SUPS and ST-VMS. Some of them have also been used in computations with the ALE-SUPS and ALE-VMS. A recent article [60] on mesh moving methods provides an overview. The general-purpose methods include, as the first one, the linear-elasticity mesh moving method with mesh-Jacobian-based stiffening [61, 62] introduced in 1992, and, as the most recent ones, element-based mesh relaxation method [63], mesh relaxation and mesh moving based on fiber-reinforced hyperelasticity [53], and back-cycle-based mesh moving method [20, 64].

With some of the most diverse and challenging classes of flow problems computed over the time period since their inception, the ST-SUPS, ALE-SUPS, RBVMS, ALE-VMS, and ST-VMS built a track record for being a powerful set of methods with wide scope. The classes of problems computed include those itemized below.

ALE-SUPS, RBVMS, and ALE-VMS:

- wind turbines [65–86],
- cardiovascular medicine [5,8,9,11,12,17,18, 31,32,87–92],
- mixed ALE-VMS/IMGA computations [9, 11, 12, 93–101] in the framework of the FSITICT,
- turbomachinery [102–108],
- two-phase flows [109–115],
- bridges [116–120],
- free-surface flows [121–125],
- IMGA FSI and flow analysis [50,126–129],
- marine applications [130–132],
- stratified flows [133,134],
- aircraft applications [135,136],
- parachutes [58],
- hypersonic flows [137],
- additive manufacturing [138].

ST-SUPS and ST-VMS:

- classes of problems summarized in [139] (all computed during the 25-year period 1993–2018),
- cardiovascular medicine [2,3,6,7,10,13–21, 140–146],
- wind turbines [4,65,72,79–82,141,142,147–154],
- parachutes [4,63,83,84,155–164],
- ground vehicles and tires [10,46,49,83,84, 165–170],
- flapping-wing aerodynamics [4, 36, 37, 60, 140–142,171–174],

- turbomachinery [47, 48, 81, 82, 175–180],
- fluid films [168, 170, 181],
- spacecraft [157, 182],
- Taylor–Couette flow [62, 183],
- disk brakes [184],
- U-ducts [185].

4. Slip (sliding) interface methods

The sliding interface method was introduced in [33, 186] in the context of the ALE-VMS. The ST version of that is the ST Slip Interface (ST-SI) method, introduced in [150]. In this article, the acronym "SI" will imply both "sliding" and "slip." Both the ALE-SI and ST-SI were introduced in the context of incompressible flows. The objective was to retain the favorable moving-mesh features of the ST-SUPS, ALE-SUPS, ALE-VMS, and ST-VMS in flow computations that have a rotating solid surface, such as a turbine rotor. The mesh around the rotating solid and inside the SI, which would typically have higher refinement near the solid surface, rotates with it and thus preserves the high-resolution boundary layer representation. The mesh outside the SI is not affected by the rotation of the solid. Connecting the two sides of the solution accurately is accomplished by adding to the ST-SUPS, ALE-SUPS, ALE-VMS, or ST-VMS formulation some integrations over the SI. The integrations, inherently residual-based, account for the velocity and stress compatibility at the SI. A number of versions of the ST-SI were introduced to serve purposes that are different than the original one but just as important.

In addition to the ST-SI version with a standard "fluid–fluid SI," a version with "fluid–solid SI" was introduced in [150]. The SI between the fluid and solid domains helps enforce the fluid mechanics Dirichlet boundary conditions weakly. The version for coupled incompressible-flow and thermal-transport equations was introduced in [184]. With that, thermo-fluid boundary layers near rotating solid surfaces can also have high-resolution representation. The version introduced in [150] has the SI between a thin porous structure and the fluid on its two sides. With that, how the porosity is dealt with is consistent with how the fluid–fluid and fluid–solid SIs are dealt with. The ST-SI versions introduced in [163] are the compressible-flow counterparts of the three versions we discussed so far. They work with the compressible-flow porosity models introduced in [163] and compressible-flow ST SUPG method [187].

The classes of problems computed with the ST-SI include turbomachinery [47, 48, 81, 82, 175–180], cardiovascular medicine [13–15, 17–21, 146], ground vehicles and tires [10, 49, 165–170], wind turbines [79–82, 150, 151], parachutes [83, 84, 162–164], fluid films [168, 170, 181], disk brakes [184], Taylor–Couette flow [183], and U-ducts [185].

5. ST Topology Change (ST-TC) method

In FSI and MBI problems, contact between moving solid surfaces can be of two types: "near contact" and actual contact. In a near contact, there is still a narrow gap between the solid surfaces, and therefore there is no topology change in the fluid mechanics domain. In such cases, the nearness is close enough for obtaining physically meaningful results from the flow computation, basically good enough for solving the problem. With a robust mesh moving method, no element needs to collapse and good boundary layer resolutions can be retained. Several classes of flow problems were computed with the ST-SUPS and ST-VMS under near-contact conditions with sufficient accuracy. Examples of such computations can be found in the references mentioned in [140].

In some classes of flow problems, it is essential to represent the contact as an actual contact. For example, in heart valve flow analysis, for obvious reasons, the contact between the valve leaflets needs to be represented as an actual contact, without leaving a narrow gap. As another example, in wing clapping aerodynamics of insects, the contact between the upper and lower wings needs to be an actual contact. The ST-

TC method [7, 140] was introduced to make ST moving-mesh computations possible even in flow problems that involve an actual contact. With that, we can both represent an actual contact and retain the good boundary layer resolution. Elements collapse as needed, which is doable in the ST context. The connectivity of the "parent" mesh, however, does not change during the process of an element collapse or rebirth, and therefore the computational efficiency does not degrade.

The ST-TC has been used without giving up neither the actual contact representation nor the high-resolution boundary layer representation in heart valve flow analysis [7, 10, 13–15, 17–19, 140, 142], ventricle-valve-aorta flow analysis [20, 21, 146], tire aerodynamics with road contact and deformation [10, 49, 165–170], fluid films [168, 170, 181], and wing clapping aerodynamics of insects [140, 174].

6. ST-SI-TC

Effective usage of the ST-TC requires its integration with the ST-SI, and the ST-SI-TC [14, 165] was introduced as that integration. We briefly summarize the need for and benefits from the ST-SI-TC. The ST-SI needs elements on both sides of a fluid–fluid SI. We need to take measures to meet that requirement in flow computations where part of the SI coincides with a solid surface. We face that, for example, when the SI is between two solid surfaces coming into contact, and in a more general context, when it merges with a fluid–solid interface. In such cases, the elements between the solid surface and the part of the SI coinciding with it collapse in the ST-TC contact mechanism. With that, the part of the SI coinciding with the solid surface switches from fluid–fluid SI to fluid–solid SI. That could create an SI that is a mixture of fluid–fluid and fluid–solid SIs. The ST-SI-TC makes the process of element collapse and rebirth independent from the nodes that represent the solid surface. The ST-SI-TC makes is possible to have high-resolution boundary layer representation near the fluid–solid interfaces even when part of the SI coincides with a solid surface. With the ST-SI-TC, we can manage contact location change and contact sliding in an effective fashion.

The ST-SI-TC has been used in heart valve flow analysis [13–15, 17–19], ventricle-valve-aorta flow analysis [20, 21, 146], tire aerodynamics with road contact and deformation [10, 49, 165–170], and fluid films [168, 170, 181].

7. ST-IGA

The ST-IGA is a broadly-defined term for the integration of the ST methods with isogeometric discretization. The method was introduced in [34]. The test computations reported in [34] were with the ST-VMS and ST-IGA and in 2D. The computations were for flow past an airfoil, with IGA basis functions in space, and for the advection equation, with IGA basis functions in both space and time. The test computations for the advection equation showed that using higher-order basis functions in time increases the accuracy return from using higher-order basis functions in space.

In early ST-IGA computations, the focus was on IGA basis function in time [34–37, 171], to have i) increased accuracy in representing the motion of solid surfaces, ii) a mesh motion consistent with that, iii) increased efficiency in representing the motion of the volume meshes, and iv) increased efficiency in remeshing. The ST/NURBS Mesh Update Method (STNMUM) [36, 37, 149, 171] was introduced possessing these desirable features. The STNMUM is suitable for, among a wider class of problems, rotating solid surfaces, and that is good context for explaining its good performance. The representation of the circular trajectory in the STNMUM is exact with the use of quadratic NURBS basis functions in time and an adequate patch count. In addition, it is possible to specify a constant angular velocity for speeds invariant along the circular trajectory. That requires a secondary mapping, given in [4, 34–36]. The "ST-C" method [188] is another positive outcome of combining the ST context with the IGA basis functions in time. It is a way of extracting a continuous representation in time from the computed data. It is also an efficient way of data

compression [10,46,81–84,152–154,175,178,179, 184,188].

The ST-IGA with IGA basis functions in time has been used in flapping-wing aerodynamics [4, 36, 37, 60, 140–142, 171–174], wind turbines [72, 79–82,141,142,149–151], turbomachinery [47,48, 81,82,175–180], and spacecraft cover separation aerodynamics [157].

Because ST-IGA with IGA basis functions in space brings increased accuracy with fewer control points and therefore larger effective element sizes, larger time-step sizes can be used while keeping the Courant number at a desirable level for good accuracy. The ST-IGA with IGA basis functions in space has been used in cardiovascular medicine [13–21, 146] turbomachinery [47, 48, 81, 82, 176–180], ground vehicles and tires [49, 166–170], wind turbines [81, 82, 151–154], parachutes [83, 84, 162, 164], fluid films [168, 170, 181], Taylor–Couette flow [183], and U-ducts [183].

The IGA basis functions in space play a key role also in the newest zero-stress-state (ZSS) estimation methods [17, 189–192] and related hyperelastic shell analysis [193]. The ZSS estimation is needed in patient-specific arterial FSI computations, because the image-based arterial geometries used in the computations do not correspond to the ZSS of the artery. The IGA basis functions in space have been used numerous advanced computational technologies in structural analysis and design, such as those reported in [194–203], including those for wind turbine blades and heart valves.

8. ST-SI-IGA and ST-SI-TC-IGA

The ST-SI-IGA [176] and ST-SI-TC-IGA [13, 14, 167] are essentially the IGA expansions of the ST-SI and ST-SI-TC discussed in Sections 4 and 6. We get ST-SI-IGA and ST-SI-TC-IGA by building an integrated combination of the ST-SI and ST-SI-TC with the ST-IGA.

The ST-SI-IGA retains the favorable moving-mesh features of the ST-SUPS, ALE-SUPS, ALE-VMS, and ST-VMS in IGA-based flow computations that have a rotating solid surface, such as a turbine rotor. The ST-SI-IGA mechanism and desirable features include those that are basically the same as what we described in Section 4. for the ST-SI. Beyond that, the ST-SI-IGA addresses the mesh generation challenge in IGA discretization. This is accomplished with an SI that does not have a slip between the two sides. The SI just connects the parts of the solution obtained over two IGA mesh zones with nonmatching meshes at the SI between the zones. Because we are no longer constrained by a matching requirement, in computation of flow problems with complex geometries, the IGA discretization becomes more practical. In IGA-based computations with a thin porous structure embedded in the flow field, the ST-SI-IGA mechanism is essentially the same as what we described in Section 4. for the ST-SI. In some cases, the rotating solid surface has grooves or creates narrow spaces or the thin porous structure has gaps and slits. In computation of such flow problems, the ST-SI-IGA makes it possible to keep the element density, and consequently the computational cost, at an acceptable level. That makes computations even with such geometric complexities practical.

The ST-SI-TC-IGA, in flow computations with contact between moving solid surfaces, makes it possible to keep the element density in the narrow spaces close to the contact region at an acceptable level. While the solid surfaces come into contact, prior to the elements between a solid surface and SI collapsing, we may have curved and complex boundaries and narrow spaces. These would need high-aspect-ratio elements. The ST-SI-TC-IGA makes it possible to compute under such adverse conditions with an acceptable level of computational cost. With the enhancements introduced in [181], the ST-SI-TC-IGA acquired a built-in Reynolds-equation limit. With that, when the solid surfaces coming into contact have fluid films between them, we do not need to use separately a Reynolds-equation model in those regions. The ST-SI-TC-IGA can handle that with comparable solution quality and computational cost and also work in the other parts of the flow domain where the Reynolds-equation model would not work.

The ST-SI-IGA and ST-SI-TC-IGA have been used in cardiovascular medicine [13–15, 17–21, 146], turbomachinery [47, 48, 81, 82, 176–180], ground vehicles and tires [49, 166–170], parachutes [83, 84, 162, 164], wind turbines [81, 82, 151], and fluid films [168, 170, 181].

9. Complex-geometry IGA mesh generation

While the IGA offers superior accuracy, IGA mesh generation for complex geometries is significantly more challenging than finite element mesh generation. Widely available mesh generation software packages for finite element and finite difference methods encourage the usage of these methods. To make IGA-based flow computations more applicable to problems with complex geometries, and consequently more practical in computational analysis of real-world problems, the IGA mesh generation will have to be less challenging and more encouraging. The Complex-Geometry IGA Mesh Generation (CGIMG) [47, 48] and NURBS Surface-to-Volume Guided Mesh Generation (NSVGMG) [49] methods were introduced to that end. We will provide a brief overview of the CGIMG here, and for the NSVGMG, we refer the interested reader to [49].

The CGIMG consists of three steps. In the first step, a block-structured mesh is generated using existing techniques for such meshes. In the second step, that mesh is projected to a NURBS mesh that is built from patches corresponding to the blocks of the block-structured mesh. In the third step, the original model surfaces are recovered, to the extent the nature of the recovered surfaces does not impede the robustness or accuracy of the flow computations. The CGIMG should normally preserve the element quality and refinement distribution of the block-structured mesh. Mesh generation and mesh quality tests were included in [47, 48]. The tests showed that the CGIMG is a practical IGA mesh generation method with good performance.

The CGIMG has been used in cardiovascular medicine [15–18, 20, 21, 48, 146], turbomachinery [47, 48, 81, 82, 107, 177, 179, 180], wind turbines [82, 151], and parachutes [48].

10. IMGA

The IMGA was first introduced in [12] as an immersed, geometrically flexible approach for solving computational FSI problems involving large, complex structural deformation and change of fluid domain topology (e.g., structural contact). The method directly analyzes a spline representation of a thin structure by immersing it into a non-body-fitted discretization of the background fluid domain and focuses on accurately capturing the immersed design geometry within a non-body-fitted analysis meshe. A new semi-implicit dynamic augmented Lagrangian (DAL) approach [204] was introduced in [12] for weakly enforcing the constraints at the fluid–structure interface in time-dependent immersogeometric FSI problems. In [12], the method was first applied to the FSI simulation of bioprosthetic heart valves (BHVs).

A mixed ALE-VMS/IMGA methodology was developed in [9] in the framework of the FSITICT [56], where a single computation combines a body-fitted, deforming-mesh treatment of some fluid–structure interfaces with a non-body-fitted treatment of others. This approach enabled us to simulate the FSI of a heart valve in a deforming artery over the entire cardiac cycle under physiological conditions and to study the effect of arterial-wall elasticity on the valve dynamics [9]. The DAL-based ALE-VMS/IMGA approach was integrated with CAD for heart valve analysis in [11] with a comparison between dynamic and FSI computations to demonstrate the importance of including FSI in heart-valve simulations. An anisotropic constitutive modeling of the BHV leaflets, based on the isogeometric Kirchhoff–Love shell formulation for general hyperelastic materials [196], was proposed in [98] and employed in the IMGA of heart-valve FSI. The framework was extended to include the coupling between the heart valve leaflets and the arterial wall in [96] to study patient-specific valve designs that do not employ stents. The results were compared with phase-contrast MRI data, in which a qualitative similarity of the flow pat-

terns in the ascending aorta was found. More recently, the framework was applied to study leaflet flutter and its potentially damaging impact on the cardiac system due to the use of thinner, more flexible biological tissues in BHVs [100, 205]. A model of a moving left ventricle was added to the heart-valve FSI framework in [101] to study the changes in the left ventricular hemodynamics following the BHV replacement of both aortic and mitral valves. In order to simulate the next generation of BHVs employed in a minimally-invasive transcatheter aortic valve replacement (TAVR) procedure, the IGA-based Bernoulli beam formulation was added to the ALE-VMS/IMGA framework in [99]. This enabled the modeling of a complex TAVR device, which includes a frame, skirt, and three leaflets, and simulation of the interaction between the blood flow, arterial wall, and TAVR in order to study the anchoring ability of the device.

Other noteworthy work on IMGA includes a divergence-conforming formulation of fluid mechanics that delivers a divergence-free velocity field everywhere in the domain and addresses the mass loss error across the valve interface [95]. In addition, clever stable coupling strategies and the appropriate definition of the Lagrange multipliers in the DAL method were proposed and analyzed in [93,94,97]. The DAL-based IMGA was also combined with surrogate modeling in [136] for the effective use of FSI to optimize the design of a hydraulic arresting gear. Parts of the IMGA methodology were recently implemented in the FEniCS-based tIGAr software [206] as a new open-source library CouDALFISh in [207]. A rigid-wall, idealized, 3D heart valve FSI example was included as part of that implementation.

11. Stabilization parameters and element lengths targeting IGA discretization

The ST-SUPS, ALE-SUPS, RBVMS, ALE-VMS, ST-VMS, like most stabilized methods, have "stabilization parameters" [4]. These parameters, which play an important role, are called "τ_{SUPG}," "τ_{PSPG}," and "ν_{LSIC}" [208]. Typically a single parameter, called "τ_{SUPS}" [4, 34], is used instead of separate τ_{SUPG} and τ_{PSPG}. A local length scale, quite often called "element length," appears in the expressions for the stabilization parameters. The element length also appears in the integrations over the SIs, with the length measured in the interface-normal direction. The expressions for the element lengths and stabilization parameters used with the ST-SUPS, ALE-SUPS, RBVMS, ALE-VMS, ST-VMS go way back to 1979–1982 [57, 209–212]. Many different expressions were introduced after that (see for example, [25, 26, 36, 46, 51, 148, 149, 213–217]), all intended, until 2018, for finite element discretization. For the first few decades, the element length was an advection length scale, measured in the flow direction, and then a second element length, which is a diffusion length scale, was added. Some of the expressions were in the ST context [25, 216], some were specific to the VMS stabilization [46], some were in the context of the coupled incompressible-flow and thermal-transport equations [46], and some made sure that element lengths, including the direction-dependent ones, had node-numbering invariance also for simplex elements [217]. All these element lengths and stabilization parameters intended for finite element discretization have also been used in computations with IGA discretization.

Element lengths and stabilization parameters targeting IGA discretization were introduced in [218]. They can also be used in computations with finite element discretization. There were three key steps in conceptually simple derivation of the direction-dependent element length expression. i) Map the direction vector from the physical ST element to the parent ST element. ii) Account for the discretization spacing along each of the parametric coordinates. iii) Map what has been obtained in the parent element back to the physical element. The latest stabilization parameters designed for the ST-VMS are those given in [167], and they are mostly from [218]. The direction-dependent element length expressions introduced in [219], which target complex-geometry B-spline meshes, are

based on a preferred parametric space instead of the standard integration parametric space. They involve a transformation tensor that represents the relationship between the two parametric spaces. These new expressions yield local length scales that are invariant with respect to element splitting (see [220] for the proof). Meeting this invariance requirement in the element length definition is essential because otherwise the solution is influenced by the element splitting, which, of course, we do not want.

The local-length-scale expressions introduced in [218, 219] have been used in ground vehicles and tires [49, 167–170], wind turbines [151–154], cardiovascular medicine [19–21, 146], fluid films [168, 181], turbomachinery [177, 180], parachutes [164], Taylor–Couette flow [183], and U-ducts [185]. They have also been used in calculating the Courant number based on the NURBS mesh local length scale in the flow direction [107]. That was in connection with an IGA-based gas turbine flow computation.

12. Constrained-Flow-Profile Traction

The Constrained-Flow-Profile (CFP) Traction [20] is an example of the special methods targeting specific classes of computations. The CFP Traction gives us flow stability at an inflow boundary where we specify not the flow velocity, as it is typically done, but the traction. The method was introduced to meet a need in computational cardiovascular medicine but can also be used in other classes of computations where we need to specify the traction at an inflow boundary.

Figure 1 shows a 2D quadratic NURBS mesh for a channel flow, which we are using as a context to describe the the CFP Traction method. We are specifying the traction at both the inflow and outflow boundaries. A large, single element placed at the inflow is the special-purpose element that serves as the core of the CFP Traction method. It has nine basis functions in 2D, and would have 27 basis functions in 3D.

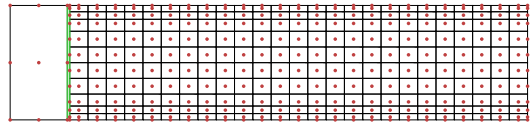

Fig. 1: CFP Traction method. The 2D quadratic NURBS mesh. The inflow boundary is on the *left*. The dots and thin lines are the control points and element boundaries. The large, single element on the *left* is the special-purpose element that serves as the core of the CFP Traction method. The two thicker lines represent the SI that connects the solutions obtained over the large element and the rest of the mesh.

An SI connect the solutions obtained over the large element and the rest of the mesh. The special-purpose element has only one unspecified control-point velocity component at the inflow boundary, and that is in the normal direction. With that configuration, a constrained flow profile is produced at the inflow boundary. It is of course a quadratic velocity profile because of the NURBS basis functions used. The combination of the quadratic velocity profile at the inflow boundary and the solution obtained for the unspecified velocity component results in the flow rate associated with the specified inflow and outflow traction values.

13. Computational example: channel flow with CFP Traction

This is a summary of the 2D test computations presented in [20]. The objective in the computations was to evaluate the performance of the CFP Traction in inflow stabilization. For this type of a test problem, computing in 2D is sufficient. We compare what we get to the analytical solution and to the solution obtained by using the outflow stabilization of [221] also at the inflow, which we will identify with the abbreviation "OS." The parameter "β" embedded in the formulation of the OS is selected from the range $\beta \geq \frac{1}{2}$ [4]. We perform three test computations. In all three, at the outflow, we use the OS with $\beta = 0.5$. Two of the test computations

are with the OS also at the inflow, and we try $\beta = 0.5$ and $\beta = 1.0$.

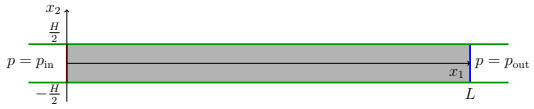

Fig. 2: Channel flow with CFP Traction. Problem setup. The parameters appearing in the figure are set as $L = 1.365\times10^{-1}$ m, $H = 1.3\times10^{-2}$ m, $p_{\text{in}} = 1.313$ Pa, and $p_{\text{out}} = 0$.

Figure 2 shows the problem setup. The density and viscosity are set as $\rho = 1{,}050$ kg/m^3 and $\mu = 4.2\times10^{-3}$ Pa·s. The channel walls have no-slip conditions. The traction conditions at the inflow and outflow are based on p_{in} and p_{out} given in Figure 2. Quadratic NURBS meshes are used in the computations. Figure 3 shows the meshes used with the OS and CFP at the inflow. The two meshes are identical everywhere in the domain other than the part covered by the special-purpose element in the CFP mesh. The number of control points and elements are 9,472 and 8,820 for the OS mesh, and 9,033 and 8,401 for the CFP mesh. The computations were performed with the ST-VMS. The time-step size was 8.6×10^{-3} s.

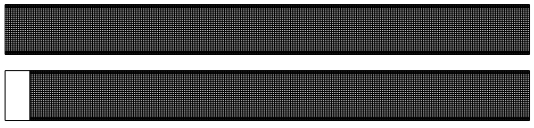

Fig. 3: Channel flow with CFP Traction. Meshes used with the OS and CFP at the inflow. The thin lines are the element boundaries. The two meshes are identical everywhere in the domain other than the part covered by the special-purpose element in the CFP mesh.

The maximum value in the parabolic velocity profile of the analytical solution is 4.84×10^{-2} m/s. The Reynolds number, defined based on that, is 157. Figure 4 shows the velocity from all three test computations. Figure 5 shows, also from all three computations, the pressure profile obtained by averaging over the channel cross-section. It is clear that the CFP Traction performs very well.

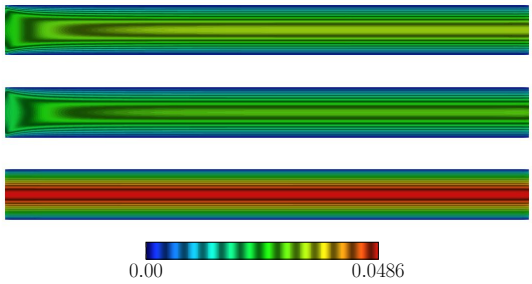

Fig. 4: Channel flow with CFP Traction. Velocity magnitude (m/s) from computations with OS ($\beta = 0.5$), OS ($\beta = 1.0$), and CFP.

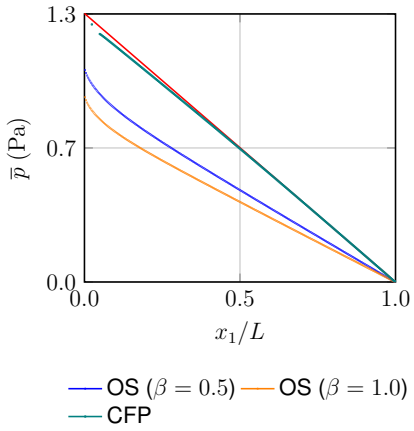

Fig. 5: Channel flow with CFP Traction. Pressure profile obtained by averaging over the channel cross-section. The analytical solution is the *red* line.

14. Computational example: flow analysis of a bioprosthetic heart valve

This flow computation of a bioprosthetic heart valve (BHV) is from [19]. It is an ST-SI-TC-IGA computation where the BHV and arterial-surface motion come from the FSI solution obtained with a mixed ALE-VMS/IMGA computation [11] in the framework of the FSITICT. In that mixed framework, the arterial surface is tracked (i.e. followed by the mesh) with the ALE-VMS, and the BHV surfaces are captured with the IMGA. The cardiac cycle is $T = 0.86$ s. The BHV model is shown in Figure 6. It has three leaflets and a metal frame. In the ALE-

VMS/IMGA computation, the BHV was represented by cubic T-splines, and the arterial surface by quadratic NURBS. Even when the valve should be closed with no gaps between the model surfaces, there were some small gaps. However, due to the nature of the IMGA computations with zero-thickness structures and limited mesh refinement, those gaps were seen as closed.

Fig. 6: Flow analysis of a BHV. Model. Leaflets, metal frame, and sinuses.

The objective in the ST-SI-TC-IGA computation was to see the model surfaces accurately, with the gaps closed, and have a high-resolution representation of the flow near those surfaces. An elaborate method was introduced in [19] to close the gaps for the ST-SI-TC-IGA computation and to have a better representation of the flow patterns near the free edges of the valve leaflets. In the ST-SI-TC-IGA computation, both the valve and arterial surfaces were represented by quadratic NURBS. Figure 7 shows the valve NURBS surfaces. Figure 8 shows the artery quadratic NURBS surfaces.

A template mesh with three SIs and three parts ("Part 1," "Part2," and "Part 3") was created in [19]. Figure 9 shows the SIs and the parts. The mesh has 429,780 control points and and 289,452 elements. Part 1 faces the SIs. It contains the elements that collapse and are reborn as the leaflets move. Its motion

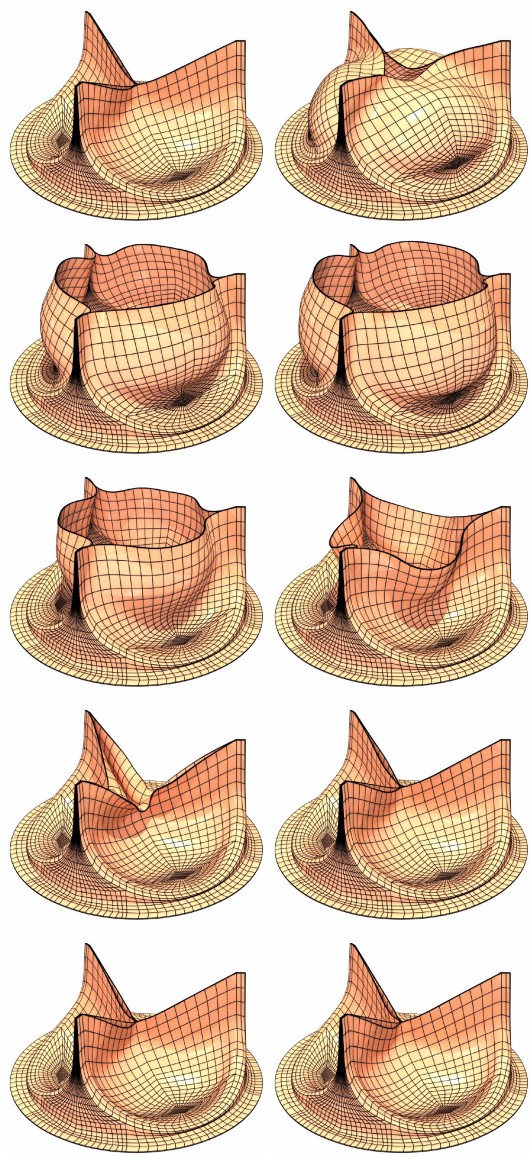

Fig. 7: Flow analysis of a BHV. Valve quadratic NURBS surfaces at t = 0.175, 0.275, 0.315, 0.495, 0.585, 0.590, 0.595, 0.605, 0.635, 0.785 s.

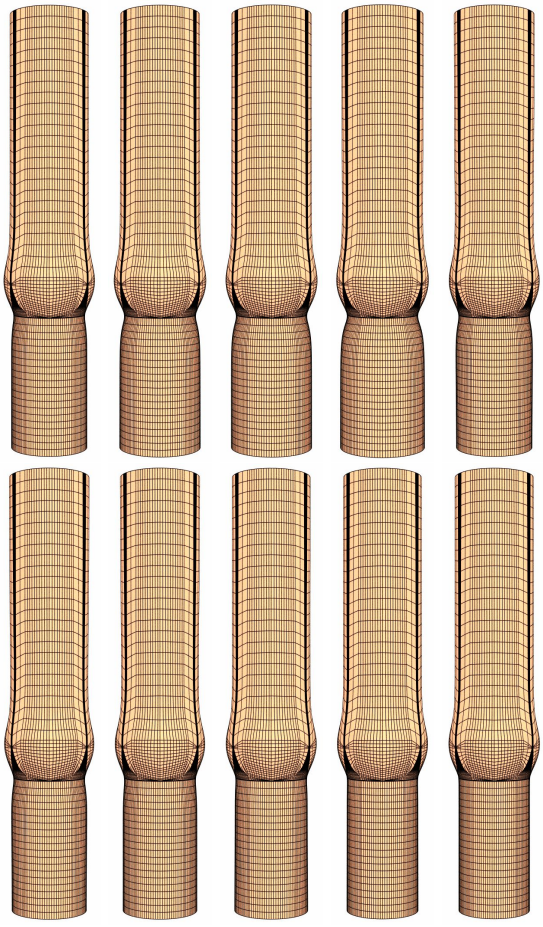

Fig. 8: Flow analysis of a BHV. Artery quadratic NURBS surfaces at $t = 0.175$, 0.275, 0.315, 0.495, 0.585, 0.590, 0.595, 0.605, 0.635, 0.785 s.

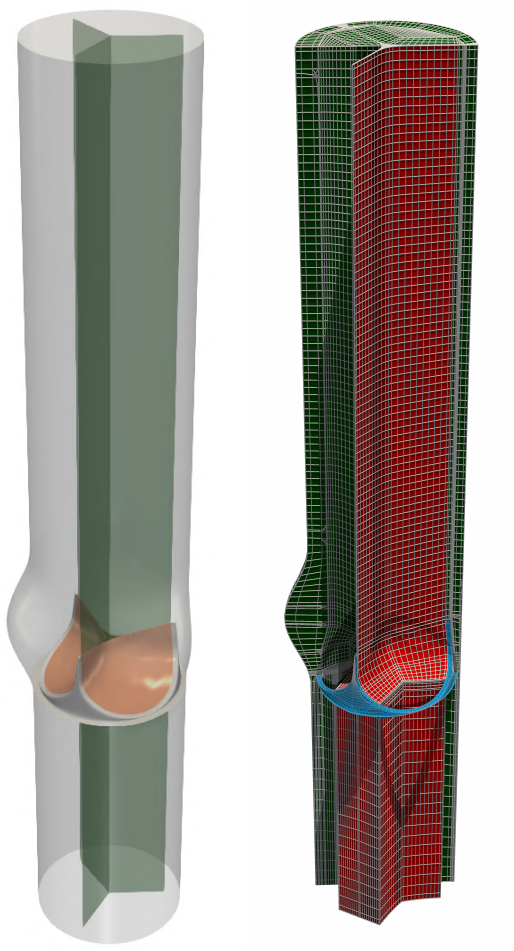

Fig. 9: Flow analysis of a BHV. Template mesh. The three SIs (*left*) and three parts (*right*): Part 1 (*red*), Part 2 (*blue*), and half of Part 3 (*green*).

is created with a special-purpose mesh moving method that takes into account the contact. Part 2 does not change during the leaflet motion. Part 3 is the rest of the mesh, between Part 1, Part 2, and the artery surface. It changes during the computation. Its motion is determined with the nonlinear-elasticity mesh moving method [46, 140, 142, 143] based on the neo-Hookean constitutive model and the mesh-Jacobian-based stiffening [4,61,62,222,223]. The motion is driven by the motion of Part 1, the valve motion, and the motion of the artery surface. Figure 10 shows the mesh motion.

The valve and the artery surface have no-slip boundary conditions, the outflow boundary is traction-free, and the inflow boundary has uniform velocity. The flow rate at the inflow is a modified version of the one in the ALE-VMS/IMGA computation. The modification makes sure that during the closed-valve part of the cardiac cycle, the inflow-boundary flow rate and the closed-space volume-change rate match. The inflow velocity corresponding to the modified flow rate, which was the velocity used in the ST-SI-TC-IGA computation, is shown in Figure 11. The computation was performed with the ST-SUPS, and the time-step size was 5.00×10^{-3} s. Figures 12 and 13 show the flow patterns during the second cardiac cycle, and Figure 14 shows the corresponding valve wall shear stress (WSS).

Fig. 10: Flow analysis of a BHV. Cross-section of the mesh at $t = 0.175$, 0.275, 0.315, 0.495, 0.585, 0.590, 0.595, 0.605, 0.635, 0.785 s. The colors are for differentiating between the NURBS patches. The checkerboard pattern is for differentiating between the elements.

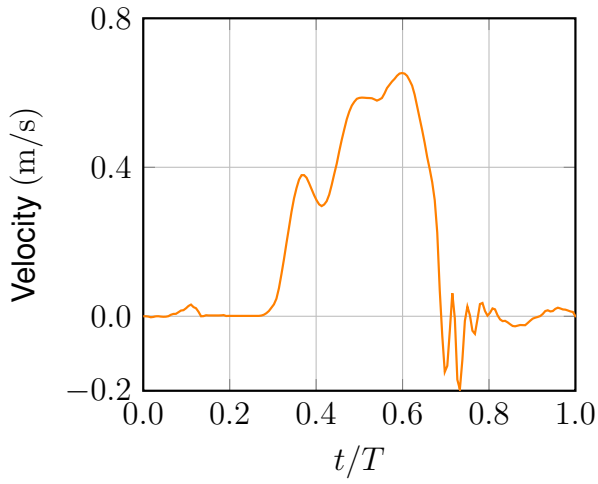

Fig. 11: Flow analysis of a BHV. Inflow velocity corresponding to the modified flow rate, which was the velocity used in the ST-SI-TC-IGA computation.

15. Computational example: FSI analysis of transcatheter aortic valve replacement

This FSI computation of a transcatheter heart valve (THV) is from [99]. Transcatheter aortic valve replacement (TAVR) is a minimally invasive alternative to open-heart valve replacement that has been increasingly used for treating various valvular diseases. The prosthetic aortic valve is deployed using a catheter and is anchored to the aortic annulus, crushing the diseased valve and assuming its function. A successful TAVR procedure depends on the proper anchoring of the THV in the aortic root of the patient. Computational FSI of TAVR offers an effective approach to understand the interaction between the THV and cardiac system and to improve THV designs for pre-operative planning. This is a mixed ALE-VMS/IMGA computation in the framework of the FSITICT, and the IGA is used in discretizing also the structural mechanics part of the FSI problem. To achieve physiological realism, the dynamics of the THV is coupled to the deforming arterial wall and the enclosed blood flow domain. The leaflets are

Fig. 12: Flow analysis of a BHV. Isosurfaces corresponding to a positive value of the second invariant of the velocity gradient tensor, colored by the velocity magnitude (m/s), at $t = 1.035$, 1.135, 1.175, 1.355, 1.445 s.

Fig. 13: Flow analysis of a BHV. Isosurfaces corresponding to a positive value of the second invariant of the velocity gradient tensor, colored by the velocity magnitude (m/s), at $t = 1.450$, 1.455, 1.465, 1.495, 1.645 s.

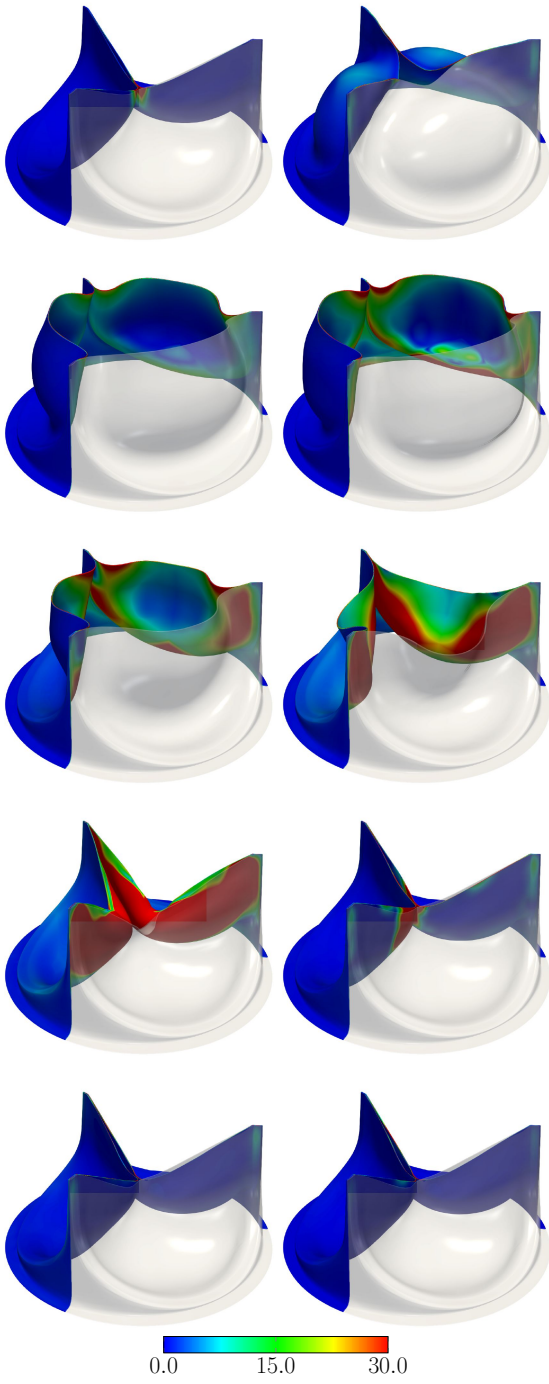

Fig. 14: Flow analysis of a BHV. Magnitude of the WSS (Pa) at t = 1.035, 1.135, 1.175, 1.355, 1.445, 1.450, 1.455, 1.465, 1.495, 1.645 s. One-third of the valve is transparent.

modeled using a transversely isotropic material that represents the mechanics of the extracellular matrix with the embedded network of collagen fibers.

A comprehensive TAVR system, the 26 mm CoreValve, was simulated in three stages in order to obtain the radial outward and friction forces between the aortic wall and the THV frame. The first stage is the crimping of THV. This is necessary since THVs are designed to have a diameter larger than that of the aortic root. During the second stage, the deployment procedure, the interaction between the THV and arterial wall is studied as the wall expands and contracts. In the third stage, the FSI simulation is employed to calculate the friction and radial forces. Their ratio is an important factor for determining the THV's anchoring ability.

Several cardiac cycles are computed until a time-periodic solution is achieved. The TAVR FSI results are shown in Figure 15. Snapshots of the detailed fluid solution fields, strain distribution, and the top view of of the valve during the cardiac cycle were plotted to illustrate the complexity of this dynamic, multiphysics system. During systole, starting at $t = 0.0$ s, the ventricular pressure is larger than the aortic pressure, which causes the valve to open and the strain to start increasing. The leaflets open and contact the frame at $t = 0.06$ s, and the valve fully opens at $t = 0.25$ s. The valve starts to close and reaches the fully closed configuration around $t = 0.38$ s. The fully loaded configuration at $t = 0.52$ s, where the maximum strain occurs, is also shown in the figure. Generally, the highest level of strain occurs during diastole when the leaflets are fully loaded. The friction force magnitude distribution is shown in Figure 16 for the fully open and fully closed configurations. In the fully closed configuration, the magnitude of the friction force is significantly larger compared to the fully opened configuration, especially around the annulus. As the valve closes and the leaflets provide a blockage for the blood flow, the magnitude of the friction force increases to counter the effect of the additional force on the THV. The coefficient of static friction is shown in Figure 17, which is defined by the ratio of the friction force to the radical force. The results indicate that the minimum of the friction coefficient, 0.22, is

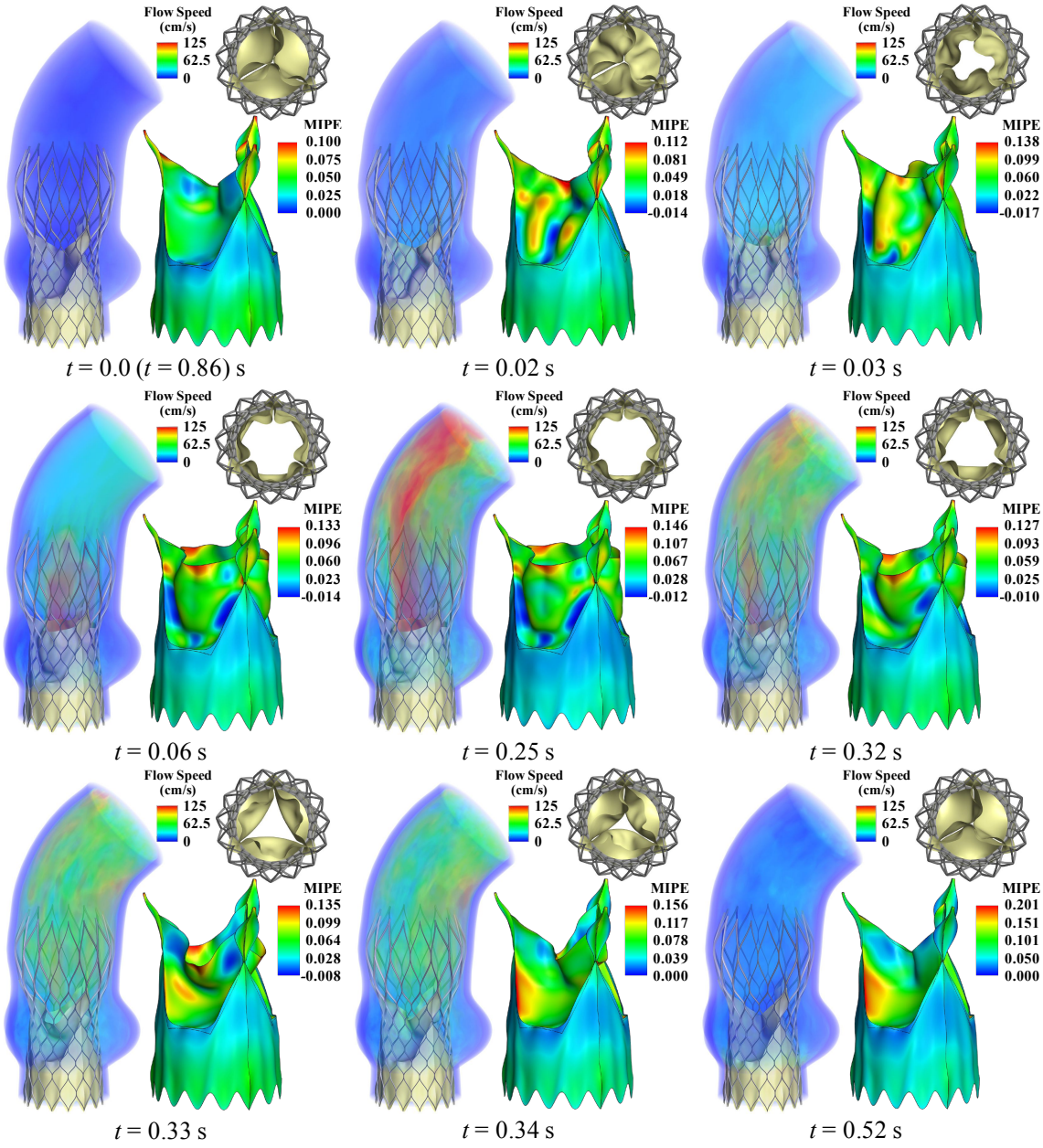

Fig. 15: Volume rendering of the velocity field at several points during a cardiac cycle. The strain map (MIPE) on the skirt and leaflets and the top view of the THV are also shown at each time. The strains are evaluated on the outer side of the shells.

necessary to anchor the TAVR without migration.

16. Concluding remarks

We have provided an overview of the IGA-based computational-cardiovascular-medicine methods built around the core methods ST-SUPS, ALE-SUPS, RBVMS, ALE-VMS, and ST-VMS.

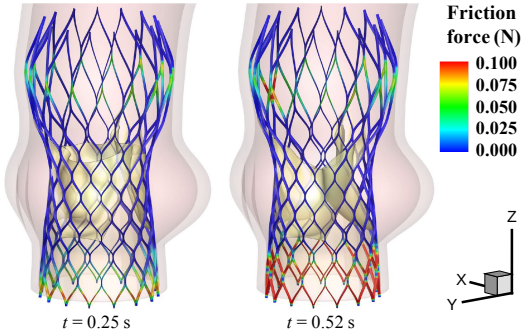

Fig. 16: The friction force magnitude distribution at the fully-opened configuration ($t = 0.25$ s) and the fully-closed configuration ($t = 0.52$ s).

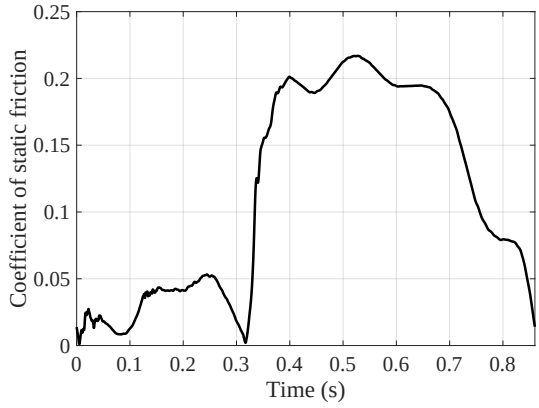

Fig. 17: Ratio of friction force magnitude to radial force magnitude over a cardiac cycle.

The superior accuracy the IGA discretization brings in both fluid and solid mechanics is in representing both the problem geometry and the variables computed. While IGA mesh generation for complex geometries is significantly more challenging than finite element mesh generation, the accuracy attained makes the effort involved in addressing that challenge worth it. We provided an overview of how the challenge has mostly been overcome with the complex-geometry mesh generation methods CGIMG and NSVGMG or circumvented with the immersed-boundary method IMGA. Quite often, specific classes of problems, such as cardiovascular medicine, require special methods targeting specific classes of computations, and we provided, as an example, an overview of one of such methods. The computational examples we presented for complex-geometry cardiovascular medicine clearly show that the advanced methods introduced have significantly increased the scope of the IGA-based computational analysis in cardiovascular medicine.

Acknowledgment

This work was supported in part by JST-CREST (first author); Grant-in-Aid for Scientific Research (A) 18H04100 from Japan Society for the Promotion of Science (first author); Rice–Waseda research agreement (first author); and Grant-in-Aid for Research Activity Start-up 16K13779 and Grant-in-Aid for Early-Career Scientists 22K17903 from Japan Society for the Promotion of Science (fifth author). The mathematical model and computational method parts of the work were also supported in part by ONR Grant N00014-21-1-2670 (second author); ARO Grant W911NF-17-1-0046 (third author) and Top Global University Project of Waseda University (third author). The second and fourth author acknowledge the Texas Advanced Computing Center (TACC) at The University of Texas at Austin for providing HPC resources that have contributed to the research results reported within this paper.

References

[1] Takizawa, K., Bazilevs, Y., & Tezduyar, T.E. (2012). Space–Time and ALE-VMS Techniques for Patient-Specific Cardiovascular Fluid–Structure Interaction Modeling. *Archives of Computational Methods in Engineering*, *19*, 171–225.

[2] Takizawa, K., Schjodt, K., Puntel, A., Kostov, N., & Tezduyar, T.E. (2012). Patient-specific computer modeling of blood flow in cerebral arteries with aneurysm and stent. *Computational Mechanics*, *50*, 675–686.

[3] Takizawa, K., Schjodt, K., Puntel, A., Kostov, N., & Tezduyar, T.E. (2013). Patient-Specific Computational Analysis of the Influence of a Stent on the Unsteady Flow in Cerebral Aneurysms. *Computational Mechanics*, *51*, 1061–1073.

[4] Bazilevs, Y., Takizawa, K., & Tezduyar, T.E. (February 2013). *Computational Fluid–Structure Interaction: Methods and Applications*. Wiley.

[5] Long, C.C., Marsden, A.L., & Bazilevs, Y. (2013). Fluid–structure interaction simulation of pulsatile ventricular assist devices. *Computational Mechanics*, *52*, 971–981.

[6] Takizawa, K., Bazilevs, Y., Tezduyar, T.E., Long, C.C., Marsden, A.L., & Schjodt, K. (2014). ST and ALE-VMS Methods for Patient-Specific Cardiovascular Fluid Mechanics Modeling. *Mathematical Models and Methods in Applied Sciences*, *24*, 2437–2486.

[7] Takizawa, K., Tezduyar, T.E., Buscher, A., & Asada, S. (2014). Space–Time Fluid Mechanics Computation of Heart Valve Models. *Computational Mechanics*, *54*, 973–986.

[8] Long, C.C., Marsden, A.L., & Bazilevs, Y. (2014). Shape optimization of pulsatile ventricular assist devices using FSI to minimize thrombotic risk. *Computational Mechanics*, *54*, 921–932.

[9] Hsu, M.C., Kamensky, D., Bazilevs, Y., Sacks, M.S., & Hughes, T.J.R. (2014). Fluid–structure interaction analysis of bioprosthetic heart valves: significance of arterial wall deformation. *Computational Mechanics*, *54*, 1055–1071.

[10] Takizawa, K. & Tezduyar, T.E. (2016). New directions in space–time computational methods. In Bazilevs, Y. & Takizawa, K. (editors), *Advances in Computational Fluid–Structure Interaction and Flow Simulation: New Methods and Challenging Computations*, Modeling and Simulation in Science, Engineering and Technology, Springer, 159–178.

[11] Hsu, M.C., Kamensky, D., Xu, F., Kiendl, J., Wang, C., Wu, M.C.H., Mineroff, J., Reali, A., Bazilevs, Y., & Sacks, M.S. (2015). Dynamic and fluid–structure interaction simulations of bioprosthetic heart valves using parametric design with T-splines and Fung-type material models. *Computational Mechanics*, *55*, 1211–1225.

[12] Kamensky, D., Hsu, M.C., Schillinger, D., Evans, J.A., Aggarwal, A., Bazilevs, Y., Sacks, M.S., & Hughes, T.J.R. (2015). An immersogeometric variational framework for fluid-structure interaction: Application to bioprosthetic heart valves. *Computer Methods in Applied Mechanics and Engineering*, *284*, 1005–1053.

[13] Takizawa, K., Tezduyar, T.E., Terahara, T., & Sasaki, T. (2018). Heart valve flow computation with the Space–Time Slip Interface Topology Change (ST-SI-TC) method and Isogeometric Analysis (IGA). In Wriggers, P. & Lenarz, T. (editors), *Biomedical Technology: Modeling, Experiments and Simulation*, Lecture Notes in Applied and Computational Mechanics, Springer, 77–99.

[14] Takizawa, K., Tezduyar, T.E., Terahara, T., & Sasaki, T. (2017). Heart valve flow computation with the integrated Space–Time VMS, Slip Interface, Topology Change and Isogeometric Discretization methods. *Computers & Fluids*, *158*, 176–188.

[15] Takizawa, K., Tezduyar, T.E., Uchikawa, H., Terahara, T., Sasaki, T., Shiozaki, K., Yoshida, A., Komiya, K., & Inoue, G. (2018). Aorta Flow Analysis and Heart Valve Flow and Structure Analysis. In Tezduyar, T.E. (editor), *Frontiers in Computational Fluid–Structure Interaction and Flow Simulation: Research from Lead Investigators under Forty – 2018*, Modeling and Simulation in Science, Engineering and Technology, Springer, 29–89.

[16] Takizawa, K., Tezduyar, T.E., Uchikawa, H., Terahara, T., Sasaki, T., & Yoshida, A. (2019). Mesh refinement influence and cardiac-cycle flow periodicity in aorta flow analysis with isogeometric discretization. *Computers & Fluids*, *179*, 790–798.

[17] Takizawa, K., Bazilevs, Y., Tezduyar, T.E., & Hsu, M.C. (2019). Computational

Cardiovascular Flow Analysis with the Variational Multiscale Methods. *Journal of Advanced Engineering and Computation*, *3*, 366–405.

[18] Hughes, T.J.R., Takizawa, K., Bazilevs, Y., Tezduyar, T.E., & Hsu, M.C. (2020). Computational Cardiovascular Analysis with the Variational Multiscale Methods and Isogeometric Discretization. In Grama, A. & Sameh, A. (editors), *Parallel Algorithms in Computational Science and Engineering*, Modeling and Simulation in Science, Engineering and Technology, Springer, 151–193.

[19] Terahara, T., Takizawa, K., Tezduyar, T.E., Bazilevs, Y., & Hsu, M.C. (2020). Heart Valve Isogeometric Sequentially-Coupled FSI Analysis with the Space–Time Topology Change Method. *Computational Mechanics*, *65*, 1167–1187.

[20] Terahara, T., Takizawa, K., Tezduyar, T.E., Tsushima, A., & Shiozaki, K. (2020). Ventricle-valve-aorta flow analysis with the Space–Time Isogeometric Discretization and Topology Change. *Computational Mechanics*, *65*, 1343–1363.

[21] Takizawa, K., Terahara, T., & Tezduyar, T.E. (2022). Space–Time Flow Computation with Contact Between the Moving Solid Surfaces. In Aldakheel, F., Hudobivnik, B., Soleimani, M., Wessels, H., Weissenfels, C., & Marino, M. (editors), *Current Trends and Open Problems in Computational Mechanics*, Springer, 517–525.

[22] Torii, R., Oshima, M., Kobayashi, T., Takagi, K., & Tezduyar, T.E. (2004). Influence of Wall Elasticity on Image-Based Blood Flow Simulations. *Transactions of the Japan Society of Mechanical Engineers Series A*, *70*, 1224–1231, in Japanese.

[23] Torii, R., Oshima, M., Kobayashi, T., Takagi, K., & Tezduyar, T.E. (2006). Computer Modeling of Cardiovascular Fluid–Structure Interactions with the Deforming-Spatial-Domain/Stabilized Space–Time Formulation. *Computer Methods in Applied Mechanics and Engineering*, *195*, 1885–1895.

[24] Tezduyar, T.E. (1992). Stabilized Finite Element Formulations for Incompressible Flow Computations. *Advances in Applied Mechanics*, *28*, 1–44.

[25] Tezduyar, T.E. (2003). Computation of Moving Boundaries and Interfaces and Stabilization Parameters. *International Journal for Numerical Methods in Fluids*, *43*, 555–575.

[26] Tezduyar, T.E. & Sathe, S. (2007). Modeling of Fluid–Structure Interactions with the Space–Time Finite Elements: Solution Techniques. *International Journal for Numerical Methods in Fluids*, *54*, 855–900.

[27] Takizawa, K., Brummer, T., Tezduyar, T.E., & Chen, P.R. (2012). A comparative study based on patient-specific fluid–structure interaction modeling of cerebral aneurysms. *Journal of Applied Mechanics*, *79*, 010908.

[28] Tezduyar, T.E., Schwaab, M., & Sathe, S. (2009). Sequentially-Coupled Arterial Fluid–Structure Interaction (SCAFSI) technique. *Computer Methods in Applied Mechanics and Engineering*, *198*, 3524–3533.

[29] Takizawa, K., Christopher, J., Tezduyar, T.E., & Sathe, S. (2010). Space–Time Finite Element Computation of Arterial Fluid–Structure Interactions with Patient-Specific Data. *International Journal for Numerical Methods in Biomedical Engineering*, *26*, 101–116.

[30] Hughes, T.J.R., Cottrell, J.A., & Bazilevs, Y. (2005). Isogeometric analysis: CAD, finite elements, NURBS, exact geometry, and mesh refinement. *Computer Methods in Applied Mechanics and Engineering*, *194*, 4135–4195.

[31] Bazilevs, Y., Calo, V.M., Zhang, Y., & Hughes, T.J.R. (2006). Isogeometric fluid–structure interaction analysis with applications to arterial blood flow. *Computational Mechanics*, *38*, 310–322.

[32] Bazilevs, Y., Calo, V.M., Hughes, T.J.R., & Zhang, Y. (2008). Isogeometric fluid–structure interaction: theory, algorithms, and computations. *Computational Mechanics*, *43*, 3–37.

[33] Bazilevs, Y. & Hughes, T.J.R. (2008). NURBS-based isogeometric analysis for the computation of flows about rotating components. *Computational Mechanics*, *43*, 143–150.

[34] Takizawa, K. & Tezduyar, T.E. (2011). Multiscale Space–Time Fluid–Structure Interaction Techniques. *Computational Mechanics*, *48*, 247–267.

[35] Takizawa, K. & Tezduyar, T.E. (2012). Space–Time Fluid–Structure Interaction Methods. *Mathematical Models and Methods in Applied Sciences*, *22*(supp02), 1230001.

[36] Takizawa, K., Henicke, B., Puntel, A., Spielman, T., & Tezduyar, T.E. (2012). Space–time computational techniques for the aerodynamics of flapping wings. *Journal of Applied Mechanics*, *79*, 010903.

[37] Takizawa, K., Henicke, B., Puntel, A., Kostov, N., & Tezduyar, T.E. (2012). Space–Time Techniques for Computational Aerodynamics Modeling of Flapping Wings of an Actual Locust. *Computational Mechanics*, *50*, 743–760.

[38] Hughes, T.J.R. (1995). Multiscale Phenomena: Green's Functions, The Dirichlet-to-Neumann Formulation, Subgrid Scale Models, Bubbles, and the Origins of Stabilized Methods. *Computer Methods in Applied Mechanics and Engineering*, *127*, 387–401.

[39] Hughes, T.J.R., Oberai, A.A., & Mazzei, L. (2001). Large Eddy Simulation of Turbulent Channel Flows by the Variational Multiscale Method. *Physics of Fluids*, *13*, 1784–1799.

[40] Bazilevs, Y., Calo, V.M., Cottrell, J.A., Hughes, T.J.R., Reali, A., & Scovazzi, G. (2007). Variational multiscale residual-based turbulence modeling for large eddy simulation of incompressible flows. *Computer Methods in Applied Mechanics and Engineering*, *197*, 173–201.

[41] Bazilevs, Y. & Akkerman, I. (2010). Large eddy simulation of turbulent Taylor–Couette flow using isogeometric analysis and the residual–based variational multiscale method. *Journal of Computational Physics*, *229*, 3402–3414.

[42] Bazilevs, Y., Hsu, M.C., Takizawa, K., & Tezduyar, T.E. (2012). ALE-VMS and ST-VMS Methods for Computer Modeling of Wind-Turbine Rotor Aerodynamics and Fluid–Structure Interaction. *Mathematical Models and Methods in Applied Sciences*, *22*(supp02), 1230002.

[43] Bazilevs, Y., Takizawa, K., & Tezduyar, T.E. (2013). Challenges and Directions in Computational Fluid–Structure Interaction. *Mathematical Models and Methods in Applied Sciences*, *23*, 215–221.

[44] Bazilevs, Y., Takizawa, K., & Tezduyar, T.E. (2015). New Directions and Challenging Computations in Fluid Dynamics Modeling with Stabilized and Multiscale Methods. *Mathematical Models and Methods in Applied Sciences*, *25*, 2217–2226.

[45] Bazilevs, Y., Takizawa, K., & Tezduyar, T.E. (2019). Computational Analysis Methods for Complex Unsteady Flow Problems. *Mathematical Models and Methods in Applied Sciences*, *29*, 825–838.

[46] Takizawa, K., Tezduyar, T.E., & Kuraishi, T. (2015). Multiscale ST Methods for Thermo-Fluid Analysis of a Ground Vehicle and its Tires. *Mathematical Models and Methods in Applied Sciences*, *25*, 2227–2255.

[47] Otoguro, Y., Takizawa, K., & Tezduyar, T.E. (2017). Space–time VMS computational flow analysis with isogeometric discretization and a general-purpose NURBS mesh generation method. *Computers & Fluids*, *158*, 189–200.

[48] Otoguro, Y., Takizawa, K., & Tezduyar, T.E. (2018). A General-Purpose NURBS

Mesh Generation Method for Complex Geometries. In Tezduyar, T.E. (editor), *Frontiers in Computational Fluid–Structure Interaction and Flow Simulation: Research from Lead Investigators under Forty – 2018*, Modeling and Simulation in Science, Engineering and Technology, Springer, 399–434.

[49] Kuraishi, T., Yamasaki, S., Takizawa, K., Tezduyar, T.E., Xu, Z., & Kaneko, R. (2022). Space–time isogeometric analysis of car and tire aerodynamics with road contact and tire deformation and rotation. *Computational Mechanics*, *70*, 49–72.

[50] Hsu, M.C., Wang, C., Xu, F., Herrema, A.J., & Krishnamurthy, A. (2016). Direct immersogeometric fluid flow analysis using B-rep CAD models. *Computer Aided Geometric Design*, *43*, 143–158.

[51] Tezduyar, T.E. (2004). Finite Element Methods for Fluid Dynamics with Moving Boundaries and Interfaces. In Stein, E., Borst, R.D., & Hughes, T.J.R. (editors), *Encyclopedia of Computational Mechanics*, Volume 3: Fluids, chapter 17, Wiley.

[52] Tezduyar, T.E., Takizawa, K., & Bazilevs, Y. (December 2017). Fluid–Structure Interaction and Flows with Moving Boundaries and Interfaces. In Stein, E., Borst, R.D., & Hughes, T.J.R. (editors), *Encyclopedia of Computational Mechanics Second Edition*, Part 2 Fluids, Wiley, published online.

[53] Takizawa, K., Tezduyar, T.E., & Avsar, R. (2020). A Low-Distortion Mesh Moving Method Based on Fiber-Reinforced Hyperelasticity and Optimized Zero-Stress State. *Computational Mechanics*, *65*, 1567–1591.

[54] Tezduyar, T., Aliabadi, S., & Behr, M. (1998). Enhanced-Discretization Interface-Capturing Technique (EDICT) for Computation of Unsteady Flows with Interfaces. *Computer Methods in Applied Mechanics and Engineering*, *155*, 235–248.

[55] Tezduyar, T.E. (2001). Finite Element Methods for Flow Problems with Moving Boundaries and Interfaces. *Archives of Computational Methods in Engineering*, *8*, 83–130.

[56] Tezduyar, T.E., Takizawa, K., Moorman, C., Wright, S., & Christopher, J. (2010). Space–Time Finite Element Computation of Complex Fluid–Structure Interactions. *International Journal for Numerical Methods in Fluids*, *64*, 1201–1218.

[57] Brooks, A.N. & Hughes, T.J.R. (1982). Streamline Upwind/Petrov-Galerkin Formulations for Convection Dominated Flows with Particular Emphasis on the Incompressible Navier-Stokes Equations. *Computer Methods in Applied Mechanics and Engineering*, *32*, 199–259.

[58] Kalro, V. & Tezduyar, T.E. (2000). A Parallel 3D Computational Method for Fluid–Structure Interactions in Parachute Systems. *Computer Methods in Applied Mechanics and Engineering*, *190*, 321–332.

[59] Hughes, T.J.R., Liu, W.K., & Zimmermann, T.K. (1981). Lagrangian–Eulerian finite element formulation for incompressible viscous flows. *Computer Methods in Applied Mechanics and Engineering*, *29*, 329–349.

[60] Takizawa, K., Bazilevs, Y., & Tezduyar, T.E. (2022). Mesh Moving Methods in Flow Computations With the Space–Time and Arbitrary Lagrangian–Eulerian Methods. *Journal of Advanced Engineering and Computation*, *6*, 85–112.

[61] Tezduyar, T.E., Behr, M., Mittal, S., & Johnson, A.A. (1992). Computation of Unsteady Incompressible Flows with the Finite Element Methods: Space–Time Formulations, Iterative Strategies and Massively Parallel Implementations. In *New Methods in Transient Analysis*, PVP-Vol.246/AMD-Vol.143, New York: ASME, 7–24.

[62] Tezduyar, T., Aliabadi, S., Behr, M., Johnson, A., & Mittal, S. (1993). Parallel

Finite-Element Computation of 3D Flows. *Computer*, *26*(10), 27–36.

[63] Takizawa, K., Tezduyar, T.E., Boben, J., Kostov, N., Boswell, C., & Buscher, A. (2013). Fluid–structure interaction modeling of clusters of spacecraft parachutes with modified geometric porosity. *Computational Mechanics*, *52*, 1351–1364.

[64] Tonon, P., Sanches, R.A.K., Takizawa, K., & Tezduyar, T.E. (2021). A linear-elasticity-based mesh moving method with no cycle-to-cycle accumulated distortion. *Computational Mechanics*, *67*, 413–434.

[65] Bazilevs, Y., Hsu, M.C., Akkerman, I., Wright, S., Takizawa, K., Henicke, B., Spielman, T., & Tezduyar, T.E. (2011). 3D Simulation of Wind Turbine Rotors at Full Scale. Part I: Geometry Modeling and Aerodynamics. *International Journal for Numerical Methods in Fluids*, *65*, 207–235.

[66] Bazilevs, Y., Hsu, M.C., Kiendl, J., Wüchner, R., & Bletzinger, K.U. (2011). 3D simulation of wind turbine rotors at full scale. Part II: Fluid–structure interaction modeling with composite blades. *International Journal for Numerical Methods in Fluids*, *65*, 236–253.

[67] Hsu, M.C., Akkerman, I., & Bazilevs, Y. (2011). High-performance computing of wind turbine aerodynamics using isogeometric analysis. *Computers & Fluids*, *49*, 93–100.

[68] Bazilevs, Y., Hsu, M.C., & Scott, M.A. (2012). Isogeometric Fluid–Structure Interaction Analysis with Emphasis on Non-Matching Discretizations, and with Application to Wind Turbines. *Computer Methods in Applied Mechanics and Engineering*, *249-252*, 28–41.

[69] Hsu, M.C., Akkerman, I., & Bazilevs, Y. (2014). Finite element simulation of wind turbine aerodynamics: Validation study using NREL Phase VI experiment. *Wind Energy*, *17*, 461–481.

[70] Korobenko, A., Hsu, M.C., Akkerman, I., Tippmann, J., & Bazilevs, Y. (2013). Structural mechanics modeling and FSI simulation of wind turbines. *Mathematical Models and Methods in Applied Sciences*, *23*, 249–272.

[71] Korobenko, A., Hsu, M.C., Akkerman, I., & Bazilevs, Y. (2013). Aerodynamic simulation of vertical-axis wind turbines. *Journal of Applied Mechanics*, *81*, 021011.

[72] Bazilevs, Y., Takizawa, K., Tezduyar, T.E., Hsu, M.C., Kostov, N., & McIntyre, S. (2014). Aerodynamic and FSI Analysis of Wind Turbines with the ALE-VMS and ST-VMS Methods. *Archives of Computational Methods in Engineering*, *21*, 359–398.

[73] Bazilevs, Y., Korobenko, A., Deng, X., Yan, J., Kinzel, M., & Dabiri, J.O. (2014). FSI modeling of vertical-axis wind turbines. *Journal of Applied Mechanics*, *81*, 081006.

[74] Bazilevs, Y., Korobenko, A., Deng, X., & Yan, J. (2015). Novel structural modeling and mesh moving techniques for advanced FSI simulation of wind turbines. *International Journal for Numerical Methods in Engineering*, *102*, 766–783.

[75] Bazilevs, Y., Korobenko, A., Yan, J., Pal, A., Gohari, S.M.I., & Sarkar, S. (2015). ALE-VMS Formulation for Stratified Turbulent Incompressible Flows with Applications. *Mathematical Models and Methods in Applied Sciences*, *25*, 2349–2375.

[76] Bazilevs, Y., Korobenko, A., Deng, X., & Yan, J. (2016). FSI modeling for fatigue-damage prediction in full-scale wind-turbine blades. *Journal of Applied Mechanics*, *83*(6), 061010.

[77] Yan, J., Korobenko, A., Deng, X., & Bazilevs, Y. (2016). Computational free-surface fluid–structure interaction with application to floating offshore wind turbines. *Computers and Fluids*, *141*, 155–174.

[78] Korobenko, A., Yan, J., Gohari, S.M.I., Sarkar, S., & Bazilevs, Y. (2017). FSI simulation of two back-to-back wind turbines

in atmospheric boundary layer flow. *Computers & Fluids*, *158*, 167–175.

[79] Korobenko, A., Bazilevs, Y., Takizawa, K., & Tezduyar, T.E. (2018). Recent Advances in ALE-VMS and ST-VMS Computational Aerodynamic and FSI Analysis of Wind Turbines. In Tezduyar, T.E. (editor), *Frontiers in Computational Fluid–Structure Interaction and Flow Simulation: Research from Lead Investigators under Forty – 2018*, Modeling and Simulation in Science, Engineering and Technology, Springer, 253–336.

[80] Korobenko, A., Bazilevs, Y., Takizawa, K., & Tezduyar, T.E. (2019). Computer modeling of wind turbines: 1. ALE-VMS and ST-VMS aerodynamic and FSI analysis. *Archives of Computational Methods in Engineering*, *26*, 1059–1099.

[81] Bazilevs, Y., Takizawa, K., Tezduyar, T.E., Hsu, M.C., Otoguro, Y., Mochizuki, H., & Wu, M.C.H. (2020). Wind Turbine and Turbomachinery Computational Analysis with the ALE and Space–Time Variational Multiscale Methods and Isogeometric Discretization. *Journal of Advanced Engineering and Computation*, *4*, 1–32.

[82] Bazilevs, Y., Takizawa, K., Tezduyar, T.E., Hsu, M.C., Otoguro, Y., Mochizuki, H., & Wu, M.C.H. (2020). ALE and Space–Time Variational Multiscale Isogeometric Analysis of Wind Turbines and Turbomachinery. In Grama, A. & Sameh, A. (editors), *Parallel Algorithms in Computational Science and Engineering*, Modeling and Simulation in Science, Engineering and Technology, Springer, 195–233.

[83] Takizawa, K., Bazilevs, Y., Tezduyar, T.E., & Korobenko, A. (2020). Variational Multiscale Flow Analysis in Aerospace, Energy and Transportation Technologies. In Grama, A. & Sameh, A. (editors), *Parallel Algorithms in Computational Science and Engineering*, Modeling and Simulation in Science, Engineering and Technology, Springer, 235–280.

[84] Takizawa, K., Bazilevs, Y., Tezduyar, T.E., & Korobenko, A. (2020). Computational Flow Analysis in Aerospace, Energy and Transportation Technologies with the Variational Multiscale Methods. *Journal of Advanced Engineering and Computation*, *4*, 83–117.

[85] Bayram, A.M., Bear, C., Bear, M., & Korobenko, A. (2020). Performance analysis of two vertical-axis hydrokinetic turbines using variational multiscale method. *Computers & Fluids*, *200*, 104432, available online.

[86] Ravensbergen, M., Bayram, A.M., & Korobenko, A. (2020). The Actuator Line Method for Wind Turbine Modelling Applied in a Variational Multiscale Framework. *Computers & Fluids*, *201*, 104465, available online.

[87] Bazilevs, Y., Gohean, J.R., Hughes, T.J.R., Moser, R.D., & Zhang, Y. (2009). Patient-specific isogeometric fluid–structure interaction analysis of thoracic aortic blood flow due to implantation of the Jarvik 2000 left ventricular assist device. *Computer Methods in Applied Mechanics and Engineering*, *198*, 3534–3550.

[88] Bazilevs, Y., Hsu, M.C., Benson, D., Sankaran, S., & Marsden, A. (2009). Computational Fluid–Structure Interaction: Methods and Application to a Total Cavopulmonary Connection. *Computational Mechanics*, *45*, 77–89.

[89] Bazilevs, Y., Hsu, M.C., Zhang, Y., Wang, W., Liang, X., Kvamsdal, T., Brekken, R., & Isaksen, J. (2010). A Fully-Coupled Fluid–Structure Interaction Simulation of Cerebral Aneurysms. *Computational Mechanics*, *46*, 3–16.

[90] Bazilevs, Y., Hsu, M.C., Zhang, Y., Wang, W., Kvamsdal, T., Hentschel, S., & Isaksen, J. (2010). Computational Fluid–Structure Interaction: Methods and Application to Cerebral Aneurysms. *Biomechanics and Modeling in Mechanobiology*, *9*, 481–498.

[91] Hsu, M.C. & Bazilevs, Y. (2011). Blood vessel tissue prestress modeling for vascular fluid–structure interaction simulations. *Finite Elements in Analysis and Design*, *47*, 593–599.

[92] Long, C.C., Esmaily-Moghadam, M., Marsden, A.L., & Bazilevs, Y. (2014). Computation of residence time in the simulation of pulsatile ventricular assist devices. *Computational Mechanics*, *54*, 911–919.

[93] Kamensky, D., Evans, J.A., & Hsu, M.C. (2015). Stability and Conservation Properties of Collocated Constraints in Immersogeometric Fluid–Thin Structure Interaction Analysis. *Communications in Computational Physics*, *18*, 1147–1180.

[94] Kamensky, D., Evans, J.A., Hsu, M.C., & Bazilevs, Y. (2017). Projection-based stabilization of interface Lagrange multipliers in immersogeometric fluid–thin structure interaction analysis, with application to heart valve modeling. *Computers and Mathematics with Applications*, *74*, 2068–2088.

[95] Kamensky, D., Hsu, M.C., Yu, Y., Evans, J.A., Sacks, M.S., & Hughes, T.J.R. (2017). Immersogeometric cardiovascular fluid–structure interaction analysis with divergence-conforming B-splines. *Computer Methods in Applied Mechanics and Engineering*, *314*, 408–472.

[96] Xu, F., Morganti, S., Zakerzadeh, R., Kamensky, D., Auricchio, F., Reali, A., Hughes, T.J.R., Sacks, M.S., & Hsu, M.C. (2018). A framework for designing patient-specific bioprosthetic heart valves using immersogeometric fluid–structure interaction analysis. *International Journal for Numerical Methods in Biomedical Engineering*, *34*, e2938.

[97] Yu, Y., Kamensky, D., Hsu, M.C., Lu, X.Y., Bazilevs, Y., & Hughes, T.J.R. (2018). Error estimates for projection-based dynamic augmented Lagrangian boundary condition enforcement, with application to fluid–structure interaction. *Mathematical Models and Methods in Applied Science*, *28*, 2457–2509.

[98] Wu, M.C.H., Zakerzadeh, R., Kamensky, D., Kiendl, J., Sacks, M.S., & Hsu, M.C. (2018). An anisotropic constitutive model for immersogeometric fluid–structure interaction analysis of bioprosthetic heart valves. *Journal of Biomechanics*, *74*, 23–31.

[99] Wu, M.C.H., Muchowski, H.M., Johnson, E.L., Rajanna, M.R., & Hsu, M.C. (2019). Immersogeometric fluid-structure interaction modeling and simulation of transcatheter aortic valve replacement. *Computer Methods in Applied Mechanics and Engineering*, *357*, 112556.

[100] Johnson, E.L., Wu, M.C.H., Xu, F., Wiese, N.M., Rajanna, M.R., Herrema, A.J., Ganapathysubramanian, B., Hughes, T.J.R., Sacks, M.S., & Hsu, M.C. (2020). Thinner biological tissues induce leaflet flutter in aortic heart valve replacements. *Proceedings of the National Academy of Sciences*, *117*, 19007–19016.

[101] Xu, F., Johnson, E.L., Wang, C., Jafari, A., Yang, C.H., Sacks, M.S., Krishnamurthy, A., & Hsu, M.C. (2021). Computational investigation of left ventricular hemodynamics following bioprosthetic aortic and mitral valve replacement. *Mechanics Research Communications*, https://doi.org/10.1016/j.mechrescom.2020.103604.

[102] Xu, F., Moutsanidis, G., Kamensky, D., Hsu, M.C., Murugan, M., Ghoshal, A., & Bazilevs, Y. (2017). Compressible flows on moving domains: Stabilized methods, weakly enforced essential boundary conditions, sliding interfaces, and application to gas-turbine modeling. *Computers & Fluids*, *158*, 201–220.

[103] Murugan, M., Ghoshal, A., Xu, F., Hsu, M.C., Bazilevs, Y., Bravo, L., & Kerner, K. (2017). Analytical Study of Articulating Turbine Rotor Blade Concept for Improved Off-Design Performance of Gas Turbine Engines. *Journal of Engineering*

for Gas Turbines and Power, *139*, 102601–6.

[104] Castorrini, A., Corsini, A., Rispoli, F., Takizawa, K., & Tezduyar, T.E. (2019). A stabilized ALE method for computational fluid–structure interaction analysis of passive morphing in turbomachinery. *Mathematical Models and Methods in Applied Sciences*, *29*, 967–994.

[105] Kozak, N., Xu, F., Rajanna, M.R., Bravo, L., Murugan, M., Ghoshal, A., Bazilevs, Y., & Hsu, M.C. (2020). High-Fidelity Finite Element Modeling and Analysis of Adaptive Gas Turbine Stator–Rotor Flow Interaction at Off-Design Conditions. *Journal of Mechanics*, *36*, 595–606.

[106] Kozak, N., Rajanna, M.R., Wu, M.C.H., Murugan, M., Bravo, L., Ghoshal, A., Hsu, M.C., & Bazilevs, Y. (2020). Optimizing Gas Turbine Performance Using the Surrogate Management Framework and High-Fidelity Flow Modeling. *Energies*, *13*, 4283.

[107] Bazilevs, Y., Takizawa, K., Wu, M.C.H., Kuraishi, T., Avsar, R., Xu, Z., & Tezduyar, T.E. (2021). Gas turbine computational flow and structure analysis with isogeometric discretization and a complex-geometry mesh generation method. *Computational Mechanics*, *67*, 57–84.

[108] Zhu, Q. & Yan, J. (2021). A moving-domain CFD solver in FEniCS with applications to tidal turbine simulations in turbulent flows. *Computers & Mathematics with Applications*, *81*, 532–546.

[109] Yan, J., Yan, W., Lin, S., & Wagner, G. (2018). A fully coupled finite element formulation for liquid–solid–gas thermo-fluid flow with melting and solidification. *Computer Methods in Applied Mechanics and Engineering*, *336*, 444–470.

[110] Yan, J., S. Lin, S., Bazilevs, Y., & Wagner, G. (2019). Isogeometric analysis of multiphase flows with surface tension and with application to dynamics of rising bubbles. *Computers & Fluids*, *179*, 777–789.

[111] Xu, S., Liu, N., & Yan, J. (2019). Residual-based variational multi-scale modeling for particle-laden gravity currents over flat and triangular wavy terrains. *Computers & Fluids*, *188*, 114–124.

[112] Bayram, A.M. & Korobenko, A. (2020). Variational Multiscale Framework for Cavitating Flows. *Computational Mechanics*, *66*, 49–67.

[113] Zhao, Z. & Yan, J. (2020). Variational multi-scale modeling of interfacial flows with a balanced-force surface tension model. *Mechanics Research Communications*, 103608.

[114] Cen, H., Zhou, Q., & Korobenko, A. (2021). Variational Multiscale Framework for Cavitating Flows. *Computers & Fluids*, *214*, 104765.

[115] Zhao, Z., Zhu, Q., & Yan, J. (2021). A thermal multi-phase flow model for directed energy deposition processes via a moving signed distance function. *Computer Methods in Applied Mechanics and Engineering*, *373*, 113518.

[116] Helgedagsrud, T.A., Bazilevs, Y., Mathisen, K.M., & Oiseth, O.A. (2019). Computational and experimental investigation of free vibration and flutter of bridge decks. *Computational Mechanics*, *63*, 121–136.

[117] Helgedagsrud, T.A., Bazilevs, Y., Korobenko, A., Mathisen, K.M., & Oiseth, O.A. (2019). Using ALE-VMS to compute aerodynamic derivatives of bridge sections. *Computers & Fluids*, *179*, 820–832.

[118] Helgedagsrud, T.A., Akkerman, I., Bazilevs, Y., Mathisen, K.M., & Oiseth, O.A. (2019). Isogeometric modeling and experimental investigation of moving-domain bridge aerodynamics. *ASCE Journal of Engineering Mechanics*, *145*, 04019026.

[119] Helgedagsrud, T.A., Bazilevs, Y., Mathisen, K.M., Yan, J., & Oiseth,

O.A. (2019). Modeling and simulation of bridge-section buffeting response in turbulent flow. *Mathematical Models and Methods in Applied Sciences*, *29*, 939–966.

[120] Helgedagsrud, T.A., Bazilevs, Y., Mathisen, K.M., & Oiseth, O.A. (2019). ALE-VMS methods for wind-resistant design of long-span bridges. *Journal of Wind Engineering and Industrial Aerodynamics*, *191*, 143–153.

[121] Akkerman, I., Bazilevs, Y., Benson, D.J., Farthing, M.W., & Kees, C.E. (2012). Free-Surface Flow and Fluid–Object Interaction Modeling with Emphasis on Ship Hydrodynamics. *Journal of Applied Mechanics*, *79*, 010905.

[122] Akkerman, I., Dunaway, J., Kvandal, J., Spinks, J., & Bazilevs, Y. (2012). Toward free-surface modeling of planing vessels: simulation of the Fridsma hull using ALE-VMS. *Computational Mechanics*, *50*, 719–727.

[123] Yan, J., Deng, X., Korobenko, A., & Bazilevs, Y. (2017). Free-surface flow modeling and simulation of horizontal-axis tidal-stream turbines. *Computers and Fluids*, *158*, 157–166.

[124] Yan, J., Deng, X., Xu, F., Xu, S., & Zhu, Q. (2020). Numerical simulations of two back-to-back horizontal axis tidal stream turbines in free-surface flows. *Journal of Applied Mechanics*, *87*(6).

[125] Zhu, Q., Yan, J., Tejada-Martínez, A., & Bazilevs, Y. (2020). Variational multiscale modeling of Langmuir turbulent boundary layers in shallow water using Isogeometric Analysis. *Mechanics Research Communications*, *108*, 103570.

[126] Xu, F., Schillinger, D., Kamensky, D., Varduhn, V., Wang, C., & Hsu, M.C. (2016). The tetrahedral finite cell method for fluids: Immersogeometric analysis of turbulent flow around complex geometries. *Computers & Fluids*, *141*, 135–154.

[127] Wang, C., Xu, F., Hsu, M.C., & Krishnamurthy, A. (2017). Rapid B-rep model preprocessing for immersogeometric analysis using analytic surfaces. *Computer Aided Geometric Design*, *52-53*, 190–204.

[128] Xu, S., Xu, F., Kommajosula, A., Hsu, M.C., & Ganapathysubramanian, B. (2019). Immersogeometric analysis of moving objects in incompressible flows. *Computers & Fluids*, *189*, 24–33.

[129] Xu, S., Gao, B., Lofquist, A., Fernando, M., Hsu, M.C., Sundar, H., & Ganapathysubramanian, B. (2020). An octree-based immersogeometric approach for modeling inertial migration of particles in channels. *Computers & Fluids*, *214*, 104764.

[130] Augier, B., Yan, J., Korobenko, A., Czarnowski, J., Ketterman, G., & Bazilevs, Y. (2015). Experimental and numerical FSI study of compliant hydrofoils. *Computational Mechanics*, *55*, 1079–1090.

[131] Yan, J., Augier, B., Korobenko, A., Czarnowski, J., Ketterman, G., & Bazilevs, Y. (2016). FSI modeling of a propulsion system based on compliant hydrofoils in a tandem configuration. *Computers and Fluids*, *141*, 201–211.

[132] Zhu, Q., Xu, F., Xu, S., Hsu, M.C., & Yan, J. (2020). An immersogeometric formulation for free-surface flows with application to marine engineering problems. *Computer Methods in Applied Mechanics and Engineering*, *361*, 112748.

[133] Yan, J., Korobenko, A., Tejada-Martinez, A.E., Golshan, R., & Bazilevs, Y. (2017). A new variational multiscale formulation for stratified incompressible turbulent flows. *Computers & Fluids*, *158*, 150–156.

[134] Ravensbergen, M., Helgedagsrud, T.A., Bazilevs, Y., & Korobenko, A. (2020). A variational multiscale framework for atmospheric turbulent flows over complex environmental terrains. *Computer Methods in Applied Mechanics and Engineering*, *368*, 113182.

[135] Wang, C., Wu, M.C.H., Xu, F., Hsu, M.C., & Bazilevs, Y. (2017). Modeling of a hydraulic arresting gear using fluid–structure interaction and isogeometric analysis. *Computers and Fluids*, *142*, 3–14.

[136] Wu, M.C.H., Kamensky, D., Wang, C., Herrema, A.J., Xu, F., Pigazzini, M.S., Verma, A., Marsden, A.L., Bazilevs, Y., & Hsu, M.C. (2017). Optimizing fluid–structure interaction systems with immersogeometric analysis and surrogate modeling: Application to a hydraulic arresting gear. *Computer Methods in Applied Mechanics and Engineering*, *316*, 668–693.

[137] Codoni, D., Moutsanidis, G., Hsu, M.C., Bazilevs, Y., Johansen, C., & Korobenko, A. (2021). Stabilized methods for high-speed compressible flows: toward hypersonic simulations. *Computational Mechanics*, *67*, 785–809.

[138] Zhu, Q., Liu, Z., & Yan, J. (2021). Machine learning for metal additive manufacturing: predicting temperature and melt pool fluid dynamics using physics-informed neural networks. *Computational Mechanics*, *67*, 619–635.

[139] Tezduyar, T.E. & Takizawa, K. (2019). Space–time computations in practical engineering applications: A summary of the 25-year history. *Computational Mechanics*, *63*, 747–753.

[140] Takizawa, K., Tezduyar, T.E., Buscher, A., & Asada, S. (2014). Space–Time Interface-Tracking with Topology Change (ST-TC). *Computational Mechanics*, *54*, 955–971.

[141] Takizawa, K., Bazilevs, Y., Tezduyar, T.E., Hsu, M.C., Øiseth, O., Mathisen, K.M., Kostov, N., & McIntyre, S. (2014). Engineering Analysis and Design with ALE-VMS and Space–Time Methods. *Archives of Computational Methods in Engineering*, *21*, 481–508.

[142] Takizawa, K. (2014). Computational Engineering Analysis with the New-Generation Space–Time Methods. *Computational Mechanics*, *54*, 193–211.

[143] Suito, H., Takizawa, K., Huynh, V.Q.H., Sze, D., & Ueda, T. (2014). FSI analysis of the blood flow and geometrical characteristics in the thoracic aorta. *Computational Mechanics*, *54*, 1035–1045.

[144] Suito, H., Takizawa, K., Huynh, V.Q.H., Sze, D., Ueda, T., & Tezduyar, T.E. (2016). A geometrical-characteristics study in patient-specific FSI analysis of blood flow in the thoracic aorta. In Bazilevs, Y. & Takizawa, K. (editors), *Advances in Computational Fluid–Structure Interaction and Flow Simulation: New Methods and Challenging Computations*, Modeling and Simulation in Science, Engineering and Technology, Springer, 379–386.

[145] Yu, Y., Zhang, Y.J., Takizawa, K., Tezduyar, T.E., & Sasaki, T. (2020). Anatomically Realistic Lumen Motion Representation in Patient-Specific Space–Time Isogeometric Flow Analysis of Coronary Arteries with Time-Dependent Medical-Image Data. *Computational Mechanics*, *65*, 395–404.

[146] Terahara, T., Kuraishi, T., Takizawa, K., & Tezduyar, T.E. (2022). Computational flow analysis with boundary layer and contact representation: II. Heart valve flow with leaflet contact. *Journal of Mechanics*, *38*, 185–194.

[147] Takizawa, K., Henicke, B., Tezduyar, T.E., Hsu, M.C., & Bazilevs, Y. (2011). Stabilized Space–Time Computation of Wind-Turbine Rotor Aerodynamics. *Computational Mechanics*, *48*, 333–344.

[148] Takizawa, K., Henicke, B., Montes, D., Tezduyar, T.E., Hsu, M.C., & Bazilevs, Y. (2011). Numerical-Performance Studies for the Stabilized Space–Time Computation of Wind-Turbine Rotor Aerodynamics. *Computational Mechanics*, *48*, 647–657.

[149] Takizawa, K., Tezduyar, T.E., McIntyre, S., Kostov, N., Kolesar, R., & Habluetzel,

C. (2014). Space–time VMS computation of wind-turbine rotor and tower aerodynamics. *Computational Mechanics*, *53*, 1–15.

[150] Takizawa, K., Tezduyar, T.E., Mochizuki, H., Hattori, H., Mei, S., Pan, L., & Montel, K. (2015). Space–time VMS method for flow computations with slip interfaces (ST-SI). *Mathematical Models and Methods in Applied Sciences*, *25*, 2377–2406.

[151] Otoguro, Y., Mochizuki, H., Takizawa, K., & Tezduyar, T.E. (2020). Space–Time Variational Multiscale Isogeometric Analysis of a tsunami-shelter vertical-axis wind turbine. *Computational Mechanics*, *66*, 1443–1460.

[152] Kuraishi, T., Zhang, F., Takizawa, K., & Tezduyar, T.E. (2021). Wind turbine wake computation with the ST-VMS method, isogeometric discretization and multidomain method: I. Computational framework. *Computational Mechanics*, *68*, 113–130.

[153] Kuraishi, T., Zhang, F., Takizawa, K., & Tezduyar, T.E. (2021). Wind turbine wake computation with the ST-VMS method, isogeometric discretization and multidomain method: II. Spatial and temporal resolution. *Computational Mechanics*, *68*, 175–184.

[154] Zhang, F., Kuraishi, T., Takizawa, K., & Tezduyar, T.E. (2022). Wind turbine wake computation with the ST-VMS method and isogeometric discretization: Directional preference in spatial refinement. *Computational Mechanics*, *69*, 1031–1040.

[155] Takizawa, K. & Tezduyar, T.E. (2012). Computational Methods for Parachute Fluid–Structure Interactions. *Archives of Computational Methods in Engineering*, *19*, 125–169.

[156] Takizawa, K., Fritze, M., Montes, D., Spielman, T., & Tezduyar, T.E. (2012). Fluid–structure interaction modeling of ringsail parachutes with disreefing and modified geometric porosity. *Computational Mechanics*, *50*, 835–854.

[157] Takizawa, K., Montes, D., Fritze, M., McIntyre, S., Boben, J., & Tezduyar, T.E. (2013). Methods for FSI modeling of spacecraft parachute dynamics and cover separation. *Mathematical Models and Methods in Applied Sciences*, *23*, 307–338.

[158] Takizawa, K., Tezduyar, T.E., Kolesar, R., Boswell, C., Kanai, T., & Montel, K. (2014). Multiscale Methods for Gore Curvature Calculations from FSI Modeling of Spacecraft Parachutes. *Computational Mechanics*, *54*, 1461–1476.

[159] Takizawa, K., Tezduyar, T.E., Boswell, C., Kolesar, R., & Montel, K. (2014). FSI Modeling of the Reefed Stages and Disreefing of the Orion Spacecraft Parachutes. *Computational Mechanics*, *54*, 1203–1220.

[160] Takizawa, K., Tezduyar, T.E., Boswell, C., Tsutsui, Y., & Montel, K. (2015). Special Methods for Aerodynamic-Moment Calculations from Parachute FSI Modeling. *Computational Mechanics*, *55*, 1059–1069.

[161] Takizawa, K., Tezduyar, T.E., & Kolesar, R. (2015). FSI Modeling of the Orion Spacecraft Drogue Parachutes. *Computational Mechanics*, *55*, 1167–1179.

[162] Takizawa, K., Tezduyar, T.E., & Terahara, T. (2016). Ram-Air Parachute Structural and Fluid Mechanics Computations with the Space–Time Isogeometric Analysis (ST-IGA). *Computers & Fluids*, *141*, 191–200.

[163] Takizawa, K., Tezduyar, T.E., & Kanai, T. (2017). Porosity models and computational methods for compressible-flow aerodynamics of parachutes with geometric porosity. *Mathematical Models and Methods in Applied Sciences*, *27*, 771–806.

[164] Kanai, T., Takizawa, K., Tezduyar, T.E., Tanaka, T., & Hartmann, A. (2019). Compressible-Flow Geometric-Porosity Modeling and Spacecraft Parachute Computation with Isogeometric Discretization. *Computational Mechanics*, *63*, 301–321.

[165] Takizawa, K., Tezduyar, T.E., Asada, S., & Kuraishi, T. (2016). Space–Time Method for Flow Computations with Slip Interfaces and Topology Changes (ST-SI-TC). *Computers & Fluids*, *141*, 124–134.

[166] Kuraishi, T., Takizawa, K., & Tezduyar, T.E. (2018). Space–Time Computational Analysis of Tire Aerodynamics with Actual Geometry, Road Contact and Tire Deformation. In Tezduyar, T.E. (editor), *Frontiers in Computational Fluid–Structure Interaction and Flow Simulation: Research from Lead Investigators under Forty – 2018*, Modeling and Simulation in Science, Engineering and Technology, Springer, 337–376.

[167] Kuraishi, T., Takizawa, K., & Tezduyar, T.E. (2019). Tire Aerodynamics with Actual Tire Geometry, Road Contact and Tire Deformation. *Computational Mechanics*, *63*, 1165–1185.

[168] Kuraishi, T., Takizawa, K., & Tezduyar, T.E. (2019). Space–Time Computational Analysis of Tire Aerodynamics with Actual Geometry, Road Contact, Tire Deformation, Road Roughness and Fluid Film. *Computational Mechanics*, *64*, 1699–1718.

[169] Tezduyar, T.E., Takizawa, K., & Kuraishi, T. (2022). Space–Time Computational FSI and Flow Analysis: 2004 and Beyond. In Aldakheel, F., Hudobivnik, B., Soleimani, M., Wessels, H., Weissenfels, C., & Marino, M. (editors), *Current Trends and Open Problems in Computational Mechanics*, Springer, 537–544.

[170] Kuraishi, T., Terahara, T., Takizawa, K., & Tezduyar, T.E. (2022). Computational flow analysis with boundary layer and contact representation: I. Tire aerodynamics with road contact. *Journal of Mechanics*, *38*, 77–87.

[171] Takizawa, K., Kostov, N., Puntel, A., Henicke, B., & Tezduyar, T.E. (2012). Space–time computational analysis of bio-inspired flapping-wing aerodynamics of a micro aerial vehicle. *Computational Mechanics*, *50*, 761–778.

[172] Takizawa, K., Henicke, B., Puntel, A., Kostov, N., & Tezduyar, T.E. (2013). Computer Modeling Techniques for Flapping-Wing Aerodynamics of a Locust. *Computers & Fluids*, *85*, 125–134.

[173] Takizawa, K., Tezduyar, T.E., & Kostov, N. (2014). Sequentially-coupled space–time FSI analysis of bio-inspired flapping-wing aerodynamics of an MAV. *Computational Mechanics*, *54*, 213–233.

[174] Takizawa, K., Tezduyar, T.E., & Buscher, A. (2015). Space–Time Computational Analysis of MAV Flapping-Wing Aerodynamics with Wing Clapping. *Computational Mechanics*, *55*, 1131–1141.

[175] Takizawa, K., Tezduyar, T.E., & Hattori, H. (2017). Computational Analysis of Flow-Driven String Dynamics in Turbomachinery. *Computers & Fluids*, *142*, 109–117.

[176] Takizawa, K., Tezduyar, T.E., Otoguro, Y., Terahara, T., Kuraishi, T., & Hattori, H. (2017). Turbocharger Flow Computations with the Space–Time Isogeometric Analysis (ST-IGA). *Computers & Fluids*, *142*, 15–20.

[177] Otoguro, Y., Takizawa, K., Tezduyar, T.E., Nagaoka, K., & Mei, S. (2019). Turbocharger turbine and exhaust manifold flow computation with the Space–Time Variational Multiscale Method and Isogeometric Analysis. *Computers & Fluids*, *179*, 764–776.

[178] Komiya, K., Kanai, T., Otoguro, Y., Kaneko, M., Hirota, K., Zhang, Y., Takizawa, K., Tezduyar, T.E., Nohmi, M., Tsuneda, T., Kawai, M., & Isono, M. (2019). Computational analysis of flow-driven string dynamics in a pump and residence time calculation. *IOP conference series earth and environmental science*, *240*, 062014.

[179] Kanai, T., Takizawa, K., Tezduyar, T.E., Komiya, K., Kaneko, M., Hirota, K., Nohmi, M., Tsuneda, T., Kawai, M., & Isono, M. (2019). Methods for Computation of Flow-Driven String Dynamics in a

Pump and Residence Time. *Mathematical Models and Methods in Applied Sciences*, *29*, 839–870.

[180] Otoguro, Y., Takizawa, K., Tezduyar, T.E., Nagaoka, K., Avsar, R., & Zhang, Y. (2019). Space–Time VMS Flow Analysis of a Turbocharger Turbine with Isogeometric Discretization: Computations with Time-Dependent and Steady-Inflow Representations of the Intake/Exhaust Cycle. *Computational Mechanics*, *64*, 1403–1419.

[181] Kuraishi, T., Takizawa, K., & Tezduyar, T.E. (2019). Space–Time Isogeometric Flow Analysis with Built-in Reynolds-Equation Limit. *Mathematical Models and Methods in Applied Sciences*, *29*, 871–904.

[182] Takizawa, K., Montes, D., McIntyre, S., & Tezduyar, T.E. (2013). Space–Time VMS Methods for Modeling of Incompressible Flows at High Reynolds Numbers. *Mathematical Models and Methods in Applied Sciences*, *23*, 223–248.

[183] Aydinbakar, L., Takizawa, K., Tezduyar, T.E., & Kuraishi, T. (2021). Space–Time VMS Isogeometric Analysis of the Taylor–Couette Flow. *Computational Mechanics*, *67*, 1515–1541.

[184] Takizawa, K., Tezduyar, T.E., Kuraishi, T., Tabata, S., & Takagi, H. (2016). Computational thermo-fluid analysis of a disk brake. *Computational Mechanics*, *57*, 965–977.

[185] Aydinbakar, L., Takizawa, K., Tezduyar, T.E., & Matsuda, D. (2021). U-duct turbulent-flow computation with the ST-VMS method and isogeometric discretization. *Computational Mechanics*, *67*, 823–843.

[186] Hsu, M.C. & Bazilevs, Y. (2012). Fluid–structure interaction modeling of wind turbines: simulating the full machine. *Computational Mechanics*, *50*, 821–833.

[187] Tezduyar, T.E., Aliabadi, S.K., Behr, M., & Mittal, S. (1994). Massively Parallel Finite Element Simulation of Compressible and Incompressible Flows. *Computer Methods in Applied Mechanics and Engineering*, *119*, 157–177.

[188] Takizawa, K. & Tezduyar, T.E. (2014). Space–time computation techniques with continuous representation in time (ST-C). *Computational Mechanics*, *53*, 91–99.

[189] Takizawa, K., Tezduyar, T.E., & Sasaki, T. (2018). Estimation of element-based zero-stress state in arterial FSI computations with isogeometric wall discretization. In Wriggers, P. & Lenarz, T. (editors), *Biomedical Technology: Modeling, Experiments and Simulation*, Lecture Notes in Applied and Computational Mechanics, Springer, 101–122.

[190] Takizawa, K., Tezduyar, T.E., & Sasaki, T. (2017). Aorta modeling with the element-based zero-stress state and isogeometric discretization. *Computational Mechanics*, *59*, 265–280.

[191] Sasaki, T., Takizawa, K., & Tezduyar, T.E. (2019). Aorta Zero-Stress State Modeling with T-Spline Discretization. *Computational Mechanics*, *63*, 1315–1331.

[192] Sasaki, T., Takizawa, K., & Tezduyar, T.E. (2019). Medical-Image-Based Aorta Modeling with Zero-Stress-State Estimation. *Computational Mechanics*, *64*, 249–271.

[193] Takizawa, K., Tezduyar, T.E., & Sasaki, T. (2019). Isogeometric hyperelastic shell analysis with out-of-plane deformation mapping. *Computational Mechanics*, *63*, 681–700.

[194] Bazilevs, Y., Hsu, M.C., Kiendl, J., & Benson, D.J. (2012). A Computational Procedure for Pre-Bending of Wind Turbine Blades. *International Journal for Numerical Methods in Engineering*, *89*, 323–336.

[195] Bazilevs, Y., Deng, X., Korobenko, A., di Scalea, F.L., Todd, M.D., & Taylor, S.G. (2015). Isogeometric fatigue damage prediction in large-scale composite structures driven by dynamic sensor data. *Journal of Applied Mechanics*, *82*, 091008.

[196] Kiendl, J., Hsu, M.C., Wu, M.C.H., & Reali, A. (2015). Isogeometric Kirchhoff–Love shell formulations for general hyperelastic materials. *Computer Methods in Applied Mechanics and Engineering*, *291*, 280–303.

[197] Hsu, M.C., Wang, C., Herrema, A.J., Schillinger, D., Ghoshal, A., & Bazilevs, Y. (2015). An interactive geometry modeling and parametric design platform for isogeometric analysis. *Computers and Mathematics with Applications*, *70*, 1481–1500.

[198] Herrema, A.J., Wiese, N.M., Darling, C.N., Ganapathysubramanian, B., Krishnamurthy, A., & Hsu, M.C. (2017). A framework for parametric design optimization using isogeometric analysis. *Computer Methods in Applied Mechanics and Engineering*, *316*, 944–965.

[199] Benzaken, J., Herrema, A.J., Hsu, M.C., & Evans, J.A. (2017). A rapid and efficient isogeometric design space exploration framework with application to structural mechanics. *Computer Methods in Applied Mechanics and Engineering*, *316*, 1215–1256.

[200] Kamensky, D., Xu, F., Lee, C.H., Yan, J., Bazilevs, Y., & Hsu, M.C. (2018). A contact formulation based on a volumetric potential: Application to isogeometric simulations of atrioventricular valves. *Computer Methods in Applied Mechanics and Engineering*, *330*, 522–546.

[201] Herrema, A.J., Johnson, E.L., Proserpio, D., Wu, M.C.H., Kiendl, J., & Hsu, M.C. (2019). Penalty coupling of non-matching isogeometric Kirchhoff–Love shell patches with application to composite wind turbine blades. *Computer Methods in Applied Mechanics and Engineering*, *346*, 810–840.

[202] Herrema, A.J., Kiendl, J., & Hsu, M.C. (2019). A framework for isogeometric-analysis-based optimization of wind turbine blade structures. *Wind Energy*, *22*, 153–170.

[203] Johnson, E.L. & Hsu, M.C. (2020). Isogeometric analysis of ice accretion on wind turbine blades. *Computational Mechanics*, *66*, 311–322.

[204] Hsu, M.C. & Kamensky, D. (2018). Immersogeometric Analysis of Bioprosthetic Heart Valves, Using the Dynamic Augmented Lagrangian Method. In Tezduyar, T.E. (editor), *Frontiers in Computational Fluid–Structure Interaction and Flow Simulation*, Cham: Springer International Publishing, 167–212.

[205] Johnson, E.L., Rajanna, M.R., Yang, C.H., & Hsu, M.C. (2022). Effects of membrane and flexural stiffnesses on aortic valve dynamics: Identifying the mechanics of leaflet flutter in thinner biological tissues. *Forces in Mechanics*, *6*, 100053.

[206] Kamensky, D. & Bazilevs, Y. (2019). tIGAr: Automating isogeometric analysis with FEniCS. *Computer Methods in Applied Mechanics and Engineering*, *344*, 477–498.

[207] Kamensky, D. (2021). Open-source immersogeometric analysis of fluid–structure interaction using FEniCS and tIGAr. *Computers & Mathematics with Applications*, *81*, 634–648.

[208] Tezduyar, T.E. & Sathe, S. (2004). Enhanced-Discretization Space-Time Technique (EDSTT). *Computer Methods in Applied Mechanics and Engineering*, *193*, 1385–1401.

[209] Hughes, T.J.R. & Brooks, A.N. (1979). A Multi-dimensional Upwind Scheme with no Crosswind Diffusion. In Hughes, T.J.R. (editor), *Finite Element Methods for Convection Dominated Flows*, AMD-Vol.34, New York: ASME, 19–35.

[210] Tezduyar, T.E. & Hughes, T.J.R. (1982). Development of Time-Accurate Finite Element Techniques for First-Order Hyperbolic Systems with Particular Emphasis on the Compressible Euler Equations. NASA Technical Report NASA-CR-204772, NASA, http://www.researchgate.net/publication/24313718/.

[211] Tezduyar, T.E. & Hughes, T.J.R. (1983). Finite Element Formulations for Convection Dominated Flows with Particular Emphasis on the Compressible Euler Equations. In *Proceedings of AIAA 21st Aerospace Sciences Meeting*, AIAA Paper 83-0125, Reno, Nevada.

[212] Hughes, T.J.R. & Tezduyar, T.E. (1984). Finite Element Methods for First-order Hyperbolic Systems with Particular Emphasis on the Compressible Euler Equations. *Computer Methods in Applied Mechanics and Engineering*, *45*, 217–284.

[213] Hughes, T.J.R., Mallet, M., & Mizukami, A. (1986). A New Finite Element Formulation for Computational Fluid Dynamics: II. Beyond SUPG. *Computer Methods in Applied Mechanics and Engineering*, *54*, 341–355.

[214] Tezduyar, T.E. & Park, Y.J. (1986). Discontinuity Capturing Finite Element Formulations for Nonlinear Convection-Diffusion-Reaction Equations. *Computer Methods in Applied Mechanics and Engineering*, *59*, 307–325.

[215] Tezduyar, T.E. & Osawa, Y. (2000). Finite Element Stabilization Parameters Computed from Element Matrices and Vectors. *Computer Methods in Applied Mechanics and Engineering*, *190*, 411–430.

[216] Tezduyar, T.E. (2001). Adaptive determination of the finite element stabilization parameters. In *Proceedings of the ECCOMAS Computational Fluid Dynamics Conference 2001 (CD-ROM)*, Swansea, Wales, United Kingdom.

[217] Takizawa, K., Ueda, Y., & Tezduyar, T.E. (2019). A Node-Numbering-Invariant Directional Length Scale for Simplex Elements. *Mathematical Models and Methods in Applied Sciences*, *29*, 2719–2753.

[218] Takizawa, K., Tezduyar, T.E., & Otoguro, Y. (2018). Stabilization and discontinuity-capturing parameters for space–time flow computations with finite element and isogeometric discretizations. *Computational Mechanics*, *62*, 1169–1186.

[219] Otoguro, Y., Takizawa, K., & Tezduyar, T.E. (2020). Element Length Calculation in B-Spline meshes for Complex Geometries. *Computational Mechanics*, *65*, 1085–1103.

[220] Ueda, Y., Otoguro, Y., Takizawa, K., & Tezduyar, T.E. (2020). Element-Splitting-Invariant Local-Length-Scale Calculation in B-Spline Meshes for Complex Geometries. *Mathematical Models and Methods in Applied Sciences*, *30*, 2139–2174.

[221] Moghadam, M.E., Bazilevs, Y., Hsia, T.Y., Vignon-Clementel, I.E., Marsden, A.L., & of Congenital Hearts Alliance (MOCHA), M. (2011). A comparison of outlet boundary treatments for prevention of backflow divergence with relevance to blood flow simulations. *Computational Mechanics*, *48*, 277–291.

[222] Johnson, A.A. & Tezduyar, T.E. (1994). Mesh Update Strategies in Parallel Finite Element Computations of Flow Problems with Moving Boundaries and Interfaces. *Computer Methods in Applied Mechanics and Engineering*, *119*, 73–94.

[223] Stein, K., Tezduyar, T., & Benney, R. (2003). Mesh Moving Techniques for Fluid–Structure Interactions with Large Displacements. *Journal of Applied Mechanics*, *70*, 58–63.

About Authors

Kenji TAKIZAWA received his PhD from Tokyo Institute of Technology in 2005, and he is currently a Professor in Department of Modern Mechanical Engineering at Waseda University. He has been conducting computational fluid mechanics research since 2000, teaching classes on that subject since 2010, and has been conducting computational FSI research since 2003. He has published over 110 Web-of-Science-indexed journal articles on computational fluid and structural mechanics and FSI. He is a Web of Science Highly Cited Researcher. He coauthored a textbook titled Computational Fluid–Structure Interaction: Methods and Applications, published by Wiley, with the Japanese translation published by Morikita Publishing Company. He served an Associate Editor of ASME Journal of Applied Mechanics and was responsible for the manuscripts on computational fluid mechanics and FSI. More information on Takizawa can be found at http://www.jp.tafsm.org/.

Yuri BAZILEVS received his PhD from University of Texas at Austin in 2006, and he is currently the E. Paul Sorensen Professor of Engineering at Brown University. He has been conducting computational fluid mechanics research since 2000, teaching classes on that subject since 2008, and has been conducting computational FSI research since 2005. He has published over 170 Web-of-Science-indexed journal articles on computational fluid and structural mechanics and FSI. He is a Web of Science Highly Cited Researcher. He coauthored a book on isogeometric analysis, a technique widely used in computational mechanics, and FSI. He coauthored a textbook titled Computational Fluid–Structure Interaction: Methods and Applications, published by Wiley, with the Japanese translation published by Morikita Publishing Company. He is an Associate Editor of Elsevier journal Computers & Fluids and is responsible for the manuscripts on computational fluid mechanics and FSI. More information on Bazilevs can be found at https://vivo.brown.edu/display/ybazilev.

Tayfun TEZDUYAR received his PhD from Caltech in 1982, and he is currently the James F. Barbour Professor of Mechanical Engineering at Rice University and Professor in Faculty of Science and Engineering at Waseda University. He has been conducting computational fluid mechanics research since 1979, teaching classes on that subject since 1987, and has been conducting computational FSI research since 1991. He has published over 260 Web-of-Science-indexed journal articles on computational fluid and structural mechanics and FSI. He is a Web of Science Highly Cited Researcher. He coauthored a textbook titled Computational Fluid–Structure Interaction: Methods and Applications, published by Wiley, with the Japanese translation published by Morikita Publishing Company. He is an Editor of Springer journal Computational Mechanics and is responsible for the manuscripts on computational fluid mechanics and FSI. More information on Tezduyar can be found at http://www.tafsm.org/tezduyar/.

Ming-Chen HSU received his PhD from University of California, San Diego in 2012, and he is currently an Associate Professor in the Department of Mechanical Engineering at Iowa State University. He has been conducting computational fluid mechanics research since 2006, teaching classes on that subject since 2013, and has been conducting computational FSI research since 2008. He has published over 80 Web-of-Science-indexed journal articles on computational fluid and structural mechanics and FSI. He is a Web of Science Highly Cited Researcher. More information on Hsu can be found at https://web.me.iastate.edu/jmchsu/.

Takuya TERAHARA received his PhD from Waseda University in 2020, and he is currently an Assistant Professor in the Department of Modern Mechanical Engineering at Waseda. He has been conducting computational fluid mechanics research since 2015. He has published 9 Web-of-Science-indexed journal articles on computational fluid and structural mechanics and FSI. More information on Terahara can be found at https://www.jp.tafsm.org/members/tterahara.